# Chapter 6

# In-Depth Analysis of the Quarter Car Suspension System using $H_\infty$ Control Synthesis

## 6.1 Introduction

A joint effort for this thesis and a final project for MAE 434: Modern Control was to analyze a design a control system for the Hyperloop's air cushion suspension system. The derivation of the system dynamics led to a very complex system that would make the design and analysis process challenging. The literature was first consulted in order to find a similar environment with a simplified system analogous to the Hyperloop's. Research on air suspension systems (Quaglia & Sorli, 2001 [45]), air cushion vehicles (Shuo et al., 2006 [50]), hovercrafts (Sira-Ramirez & Ibanez, 2000 [52]) and maglev systems (Cai & Chen, 1996 [7]) revealed models that either did not fit with the Hyperloop's or remained too large of scope to effectively navigate the system. While considering alternative models, the quarter car suspension system appeared quite frequently. Although there were some key differences between this model and that of the Hyperloop's suspension system, the model is simple to analyze and there is the opportunity to gain basic understanding of the suspension concept and later translate the findings to the Hyperloop's system. Stable operation and acceptable ride comfort requires vehicle motion control in both cases. Passive systems only store or dissipate energy associated with vibration. This is insufficient to improve the performance

requirements and be robust to road roughness and other transient disturbing forces. Therefore, an active suspension system is needed. For the quarter car suspension system $H_\infty$ techniques were first used to design a controller for the nominal model. Then, $\mu$ synthesis was explored to design a controller that was robust to uncertainty in the model.

## 6.2 Quarter Car Suspension Model

The quarter car suspension system can be modeled as a one-dimensional vehicle with two degrees of freedom (Figure 6.1). The mass of the capsule's body (chassis) is represented by $m_b$ and the mass of the wheel assembly (air bearing ski) is $m_w$. Between the capsule body and the wheel assembly there is a passive spring, $k_s$, and a shock absorber (damper), $b_s$. The compressibility of the pneumatic tire (the air cushion) can be modeled by $k_t$. The active component of the suspension system is an applied force, $f_s$, applied between the body and the wheel assembly, while the compressor force, $f_{comp}$, is applied between the wheel assembly and the road (tube bottom wall). In the literature there were other models found for this system. The main differences were an additional damper in the wheel assembly and moving the location of the applied force to between the road and the wheel assembly. To simplify this system in order to observe the overall control effect on road handling and comfort, the compressor force will not be considered as an actuated force. Thus, the only actuated force input will be, $f_s$.

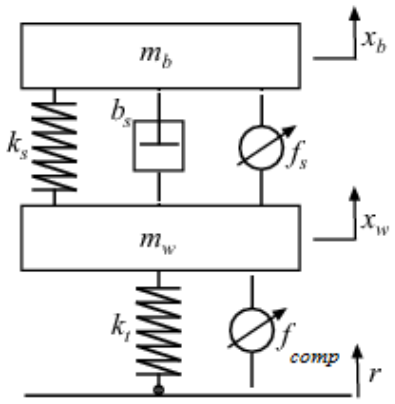



Figure 6.1: Quarter Car Suspension Model

The equations of motion when the vehicle is at an equilibrium position are

$$m_w\ddot{x}_w + k_t(x_w - r) - b_s(\dot{x}_b - \dot{x}_w) - k_s(x_b - x_w) = -f_s \tag{6.2.1}$$

$$m_b\ddot{x}_b + b_s(\dot{x}_b - \dot{x}_w) + k_s(x_b - x_w) = f_s \tag{6.2.2}$$

Define the follow states: $x_1 = x_b$, $x_2 = \dot{x}_1 = \dot{x}_b$, $x_3 = x_w$, and $x_4 = \dot{x}_3 = \dot{x}_w$.

This leads to the following state-space equations.

$$\begin{aligned}
\dot{x}_1 &= x_2 \\
\dot{x}_2 &= -\frac{1}{m_b}[k_s(x_1 - x_3) + b_s(x_2 - x_4) - f_s] \\
\dot{x}_3 &= x_4 \\
\dot{x}_4 &= \frac{1}{m_w}[k_s(x_1 - x_3) + b_s(x_2 - x_4) - k_t(x_3 - r) - f_s]
\end{aligned}$$

The continuous-time LTI system is defined by

$$\begin{aligned}
\dot{x}(t) &= Ax(t) + Bu(t) \\
y(t) &= Cx(t) + Du(t)
\end{aligned}$$

where,

$$A = \begin{bmatrix} 0 & 1 & 0 & 0 \\ \frac{-k_s}{m_b} & \frac{-b_s}{m_b} & \frac{k_s}{m_b} & \frac{b_s}{m_b} \\ 0 & 0 & 0 & 1 \\ \frac{k_s}{m_w} & \frac{b_s}{m_w} & \frac{-k_s-k_t}{m_w} & \frac{-b_s}{m_w} \end{bmatrix}, \quad B = \begin{bmatrix} 0 & 0 \\ 0 & \frac{f_s}{m_b} \\ 0 & 0 \\ \frac{k_t}{m_w} & \frac{-f_s}{m_w} \end{bmatrix},$$

$$C = \begin{bmatrix} 1 & 0 & 0 & 0 \\ 1 & 0 & -1 & 0 \\ \frac{-k_s}{m_b} & \frac{-b_s}{m_b} & \frac{k_s}{m_b} & \frac{b_s}{m_b} \end{bmatrix}, \text{ and } \quad D = \begin{bmatrix} 0 & 0 \\ 0 & 0 \\ 0 & \frac{f_s - f_{comp}}{m_b} \end{bmatrix}$$

The model inputs are the road disturbance, $r$, and the actuator force, $f_s$.

The model outputs are the car body travel, $x_b$, the suspension deflection, $s_d = x_b - x_w$,

and the capsule's body's acceleration, $a_b = \ddot{x}_b$. It is apparent that there will be a tradeoff between good handling of the system (small $s_d$) and high passenger comfort (small $a_b$).

The parameter values are mostly taken from the Hyperloop alpha system assuming 28 air bearing suspension skis while the damping and spring constants were adapted from Roinila (2011) and MathWorks (2013) [47] [30] (Table 6.1).

| System Parameter | Value |
|---|---|
| $m_b$ (kg) | 425.0 |
| $m_w$ (kg) | 110.7 |
| $b_s$ (N/m/s) | 100 |
| $k_s$ (N/m) | 16000 |
| $k_t$ (N/m) | 190000 |

Table 6.1: Hyperloop Parameters for Quarter Car Suspension Model

## 6.3 Hydraulic Actuator Model

A hydraulic actuator connected between the body mass and wheel assembly mass is used for active suspension control. There are five main components: the electro hydraulic powered spool valve, piston-cylinder, hydraulic pump, reservoir, and piping system (Figure 6.2). The actuator considered has a max displacement of 0.05 meters [30]. The nominal model is an approximation of the physical actuator dynamics and can be represented by the transfer function,

$$Act_{Nominal} = \frac{1}{\frac{1}{60}s + 1}$$

This is similar to transfer function for servo motors with form

$$T_f = K\frac{1}{\tau s + 1}$$

where $K$ is the servo valve static flow gain at zero load pressure drop and $\tau$ is the apparent servo valve time constant [57]. If a wider frequency range is desired, a second order response can be used.

Model variations in the actuator are considered for the robustness analysis.

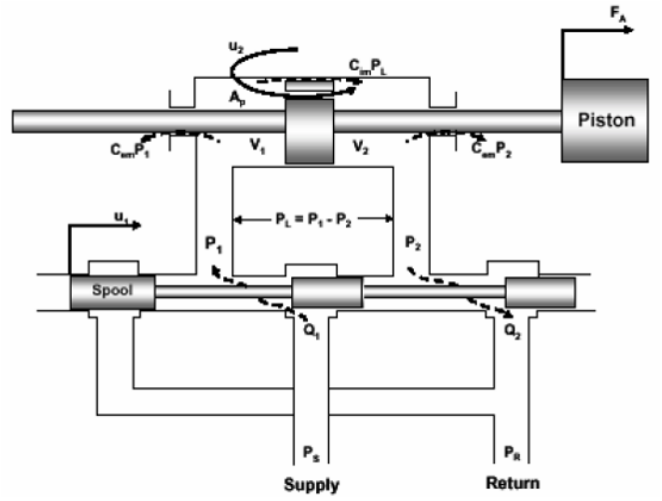



Figure 6.2: Hydraulic Actuator

## 6.4 Preliminary Analysis

Preliminary analysis began with determining the matrix A is Hurwitz, as well as investigating the controllability, stabilizability, detectability, and other properties of the system. For this analysis, two properties were of importance. The zeroes of the transfer function from the actuator to the body travel and acceleration have an imaginary-axis zero. The natural frequency of this zero is called the tire-hop frequency (41.43 rad/s). The imaginary-axis zero for the transfer function from the actuator to the suspension defelction is called the rattlespace frequency (18.83 rad/s). These can be observed in the Bode plots for these transfer functions (Figure 6.3). The quick spike down for the actuator force curves (red) reveal these special frequencies. Feedback control cannot improve the response from road disturbance to body acceleration at the tire hop frequency. And likewise, it cannot improve the response from road disturbance to suspension deflection at the rattlespace frequency.

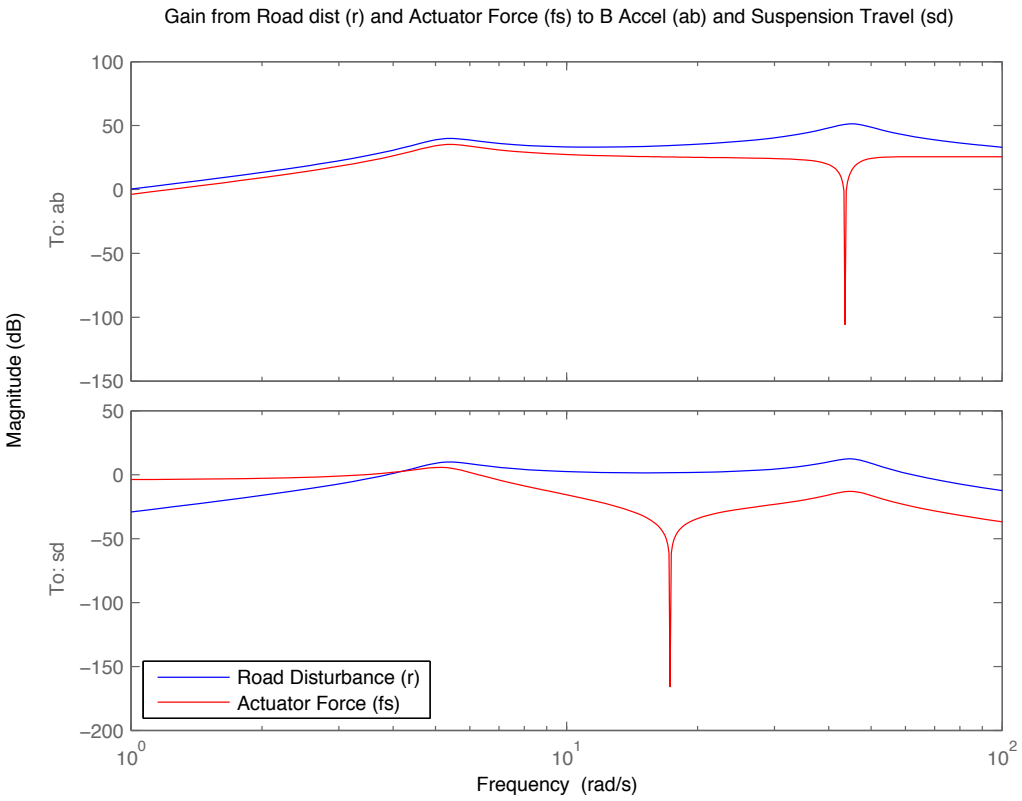



Figure 6.3: Bode Plot Showing the Tire Hop and Rattlespace Frequencies

## 6.5 $H_\infty$ Control Synthesis

The goal of $H_\infty$ methods is to synthesize a controller that minimizes a single cost function. The optimization considers factors such as passenger comfort, road handling, quality of sensor measurements for feedback, and possible limits on available control force. Weighted parameters are used to model external disturbances and emphasize design objectives. The optimization takes place over the Banach space $H_\infty$, which consists of all complex-valued functions of a complex variable which are analytic and bounded in the open right-half complex plane defined by $Re(s) > 0$. The $H_\infty$ norm is the maximum singular value over this space (peak gain). The synthesis can be used to minimize the closed-loop impact of perturbations.

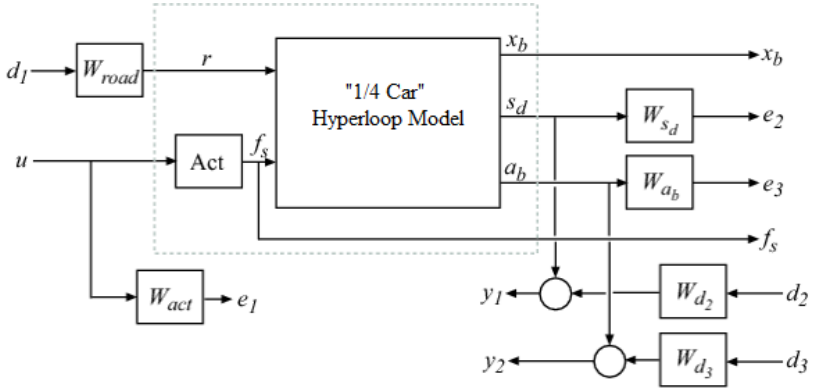



Figure 6.4: $H_\infty$ model for Quarter Car Suspension System

The control objectives can be understood as disturbance rejection of the disturbance signals $d_1$, $d_2$, and $d_3$ (Figure 6.4). The road disturbance is modeled by the normalized signal, $d_1$, and is shaped by the weighting function,$W_{road}$. $d_2$ and $d_3$ represent the normalized signals of the noise on the measurements $y_1$ and $y_2$ (suspension travel and body acceleration respectively). These measurements are used by the feedback controller to compute the control signal, $u$, which drives the hydraulic actuator. They are shaped by the weighting functions $W_{d_2}$ and $W_{d_3}$. The $H_\infty$ design minimizes the impact of these disturbances according to the weights specified. The weights are set by the goals of the suspension travel, body acceleration, and control effort. The designed controller then minimizes the $H_\infty$ norm from the disturbance inputs to the error signals ($e_1$, $e_2$, and $e_3$).

The weights used were taken from a combination of Roinila (2011) and MathWorks (2013) [47] [30]. $W_{road}$ was set to model broadband road deflections of magnitude 7 mm. A high-pass filter that penalizes the high-frequency of the control signal and

[6]MATLAB analysis adapted from [47] [30] [31]

limits the control bandwidth is used for $W_{act}$. The weighting functions $W_{d_2}$ and $W_{d_3}$ were adjusted to model broadband senor noise.

Target transfer functions for the closed-loop response of the system were established to represent goals of passenger comfort and adequate road handling. These were used to help determine the weighting functions ($W_{s_d}$ and $W_{a_b}$ are reciprocals of the comfort and handling targets). The target transfer functions are plotted vs. the open-loop response for the road disturbance to the suspension deflection and body acceleration in Figure 6.5.

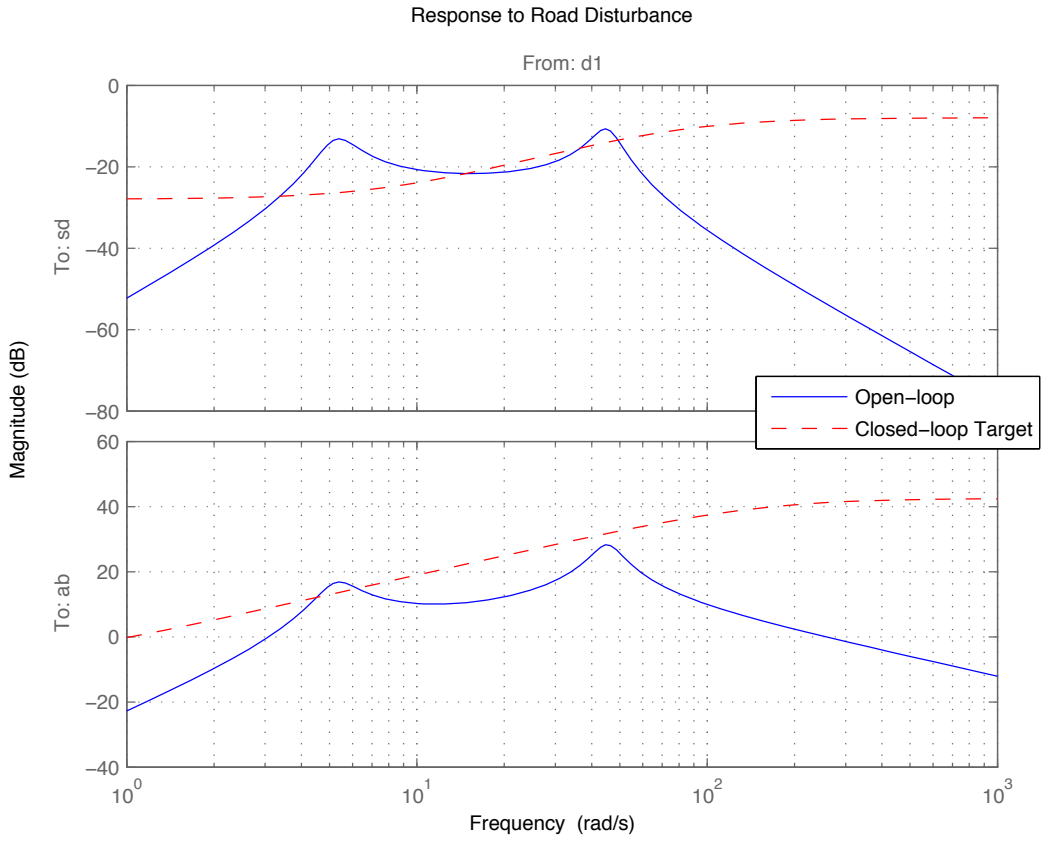



Figure 6.5: Target Closed-Loop Response vs. Open-Loop Response

The tradeoffs between passenger comfort and handling can be explored by creating a blending parameter, $\beta$, that modulates the tradeoff. The $\beta$ parameter was then used to create separate controller models. Three separate cases were established: emphasize comfort ($\beta = 0.1$), emphasize handling ($\beta = 0.9$), and a balance between comfort and handling ($\beta = 0.5$). Then weights were calculated corresponding to each case using $W_{s_d} = \frac{\beta}{HandlingTarget}$ and $W_{a_b} = \frac{1-\beta}{ComfortTarget}$.

The MATLAB command hinfsyn(P,NMEAS,NCON) was used to compute the $H_\infty$ controller K for plant P, number of measurement outputs, NMEAS, and number of control inputs, NCON. The MATLAB function ignores the uncertainty in the plant model and, thus, a controller is synthesized for only the nominal value of each model. The weighted plant model's control input for the quarter car system is the hydraulic actuator force and the two measurement outputs are those for the suspension deflection and body acceleration. The closed-loop $H_\infty$ norms are displayed in Table 6.2. Using the designed controller for each blending parameter, $\beta$, the closed-loop model was constructed. The frequency response is plotted in Figure 6.6 and compared to the passive suspension system (open-loop). All three cases show reductions for suspension deflection and body acceleration below the rattlespace frequency.

| $\beta$ Condition | $H_\infty$ norm |
|---|---|
| $\beta = 0.1$ (Comfort) | 0.632 |
| $\beta = 0.9$ (Handling) | 0.766 |
| $\beta = 0.5$ (Balance) | 1.066 |

Table 6.2: $H_\infty$ Norm for Various $\beta$ Conditions

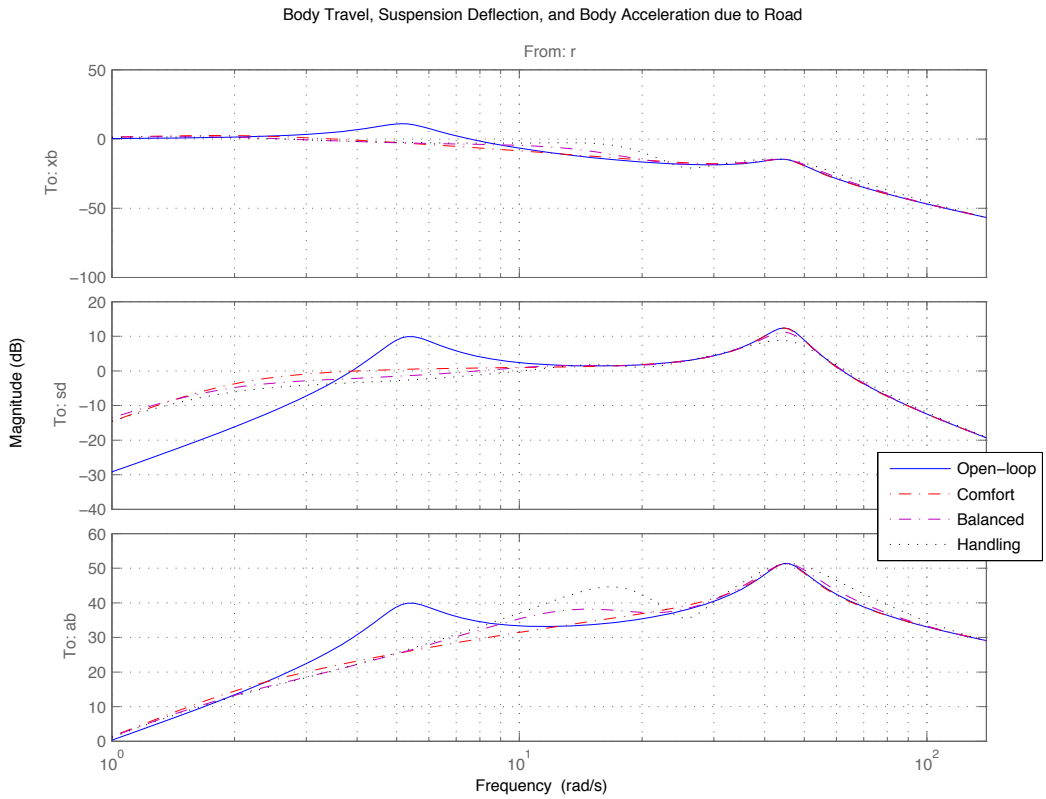



Figure 6.6: Closed-loop for $H_\infty$ synthesized controllers for each blending parameter, $\beta$, compared to passive suspension system (open-loop)

The effect of the blending parameter, $\beta$, for the design of the $H_\infty$ controller is more easily observed in the time response. Figure 6.7 shows simulations for a road (tube surface) disturbance signal (green curve) characterized by,

$$r(t) = \begin{cases} .0005(1 - cos(8\pi t) & , 0 \leq t \leq 0.25 \\ 0 & , \ otherwise \end{cases}$$

The tradeoffs of comfort and handling are very evident. For example, the body acceleration is the smallest for the controller emphasizing comfort (red curve) and is the largest for the controller emphasizing handling (black curve). The suspension deflection is minimized for the handling case and is worse for the comfort case. However, the controller that balances the goals actually provides a very good compromise for all responses (pink curve). This would be the recommended controller to use.

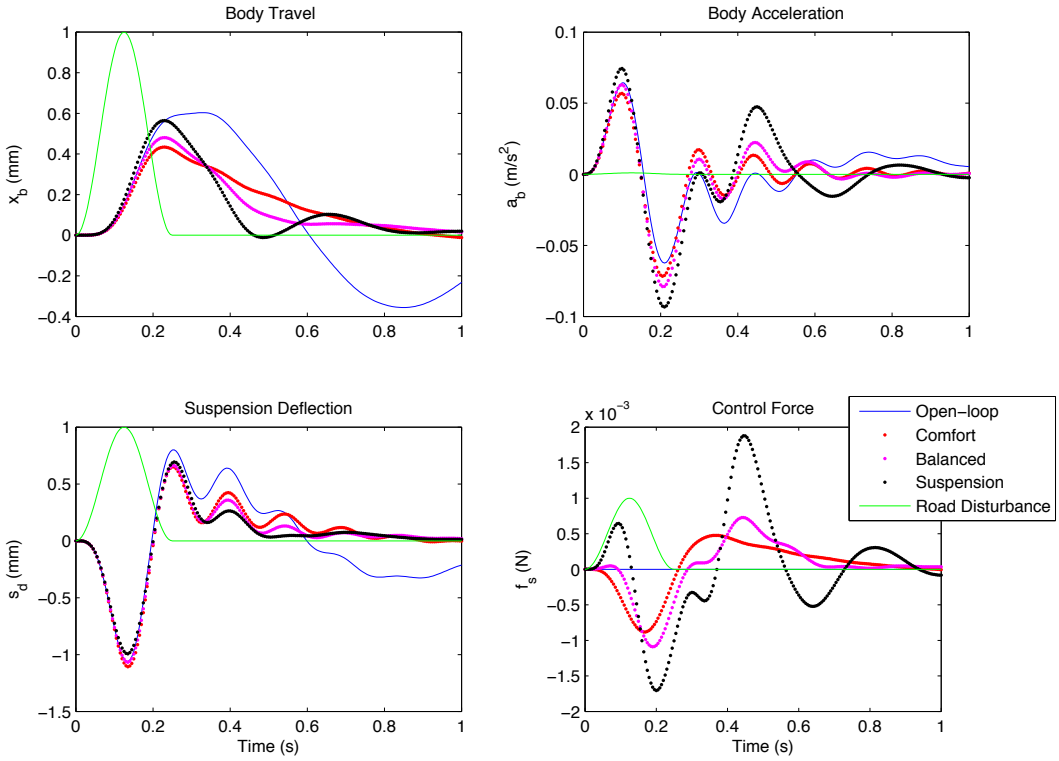



Figure 6.7: Time Response for Road Disturbance Signal: Effect of Blending Parameter, $\beta$

## 6.6 Robust $\mu$ Synthesis

The $H_\infty$ controller was constructed for only the nominal actuator model, which is an approximation of the true actuator. The design needs some further work to ensure performance is maintained even with model error and uncertainty. The robust controller was synthesized using D-K iteration for the model with actuator uncertainty. The MATLAB command dksyn(P,NMEAS,NCONT) synthesizes a controller K for the open-loop plant model P via the D-K iteration approach to $\mu$-synthesis. P is a state-space model with uncertainty incorporated and it is assumed that the last NMEAS outputs and NCONT inputs of P are the measurement and control channels, respectively. The balanced model case was examined. The closed-loop response for the robust design is compared to the open-loop (Figure 6.8). The responses are very similar to the balanced $H_\infty$-only controller in the absence of uncertainties.

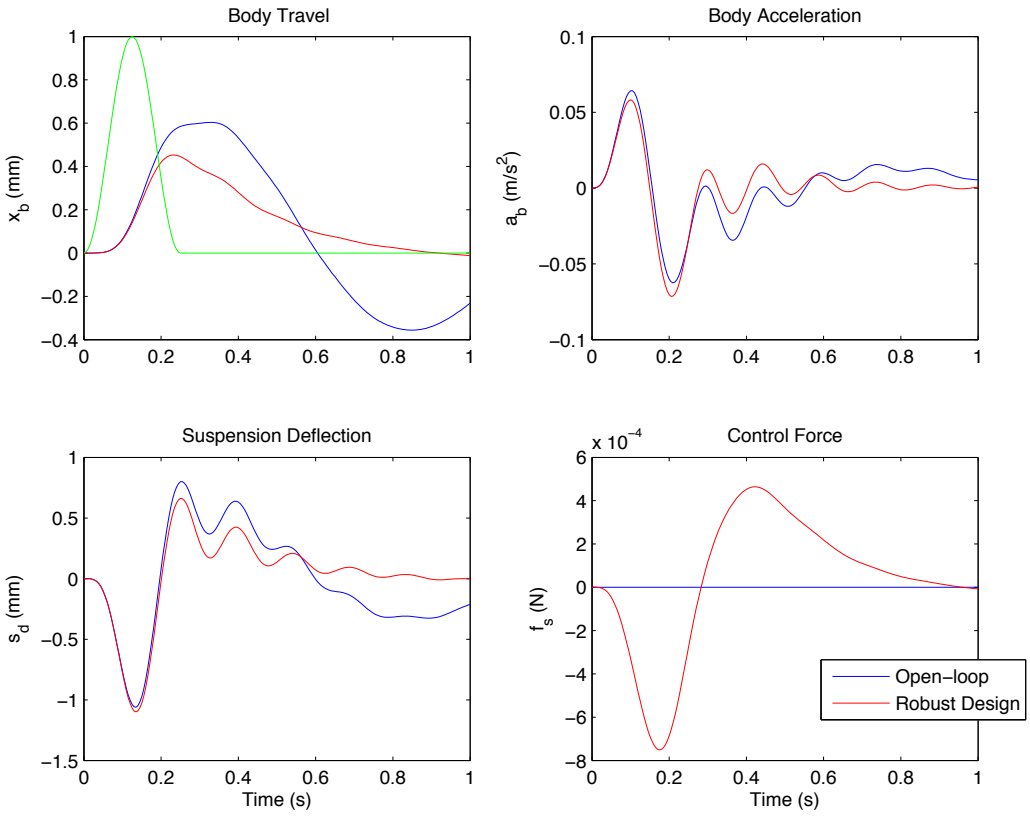



Figure 6.8: Time Response for Road Disturbance Signal: Robust $\mu$ Synthesized Controller vs. Open-Loop.

Variability caused by model uncertainty was used to determine the effectiveness of the robust controller. The response to the road bump was simulated for 120 randomly sampled actuator models from the uncertainty model. When these simulations are run for the $H_\infty$ only controller (nominal model), the response is quite noisy. This is depicted by the deviation of the closed-loop with uncertainties (the blue curves) from the nominal closed-loop (red curve) in Figure 6.9. The same simulation was run for the $\mu$ synthesized balanced robust controller (Figure 6.10) and the variability was significantly reduced.

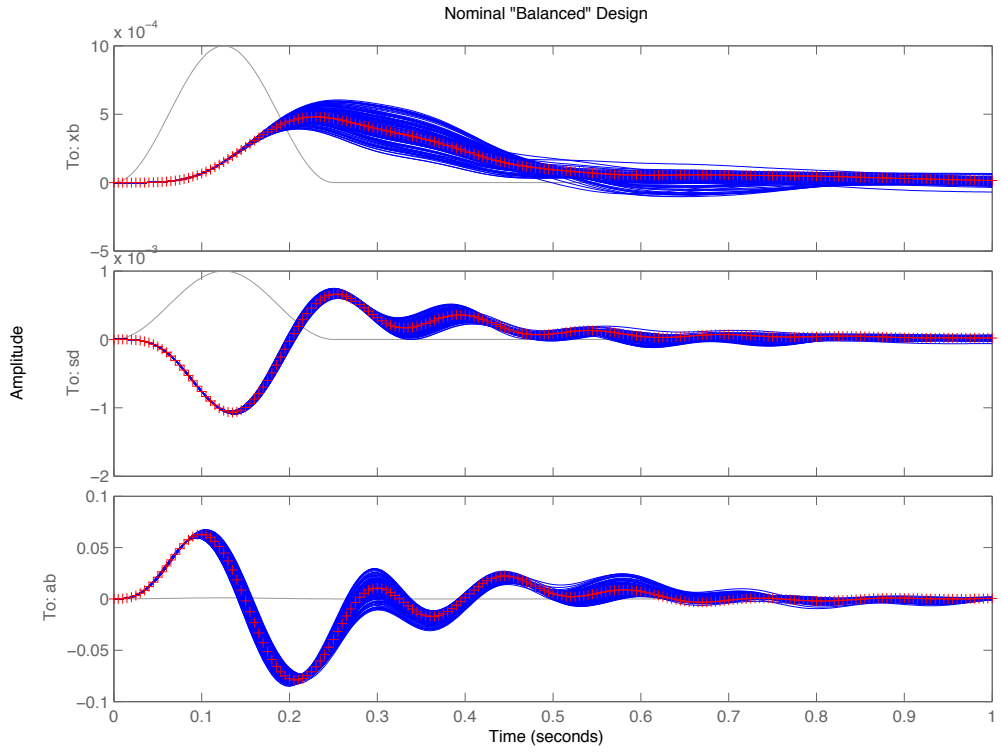



Figure 6.9: Time Response for Road Disturbance Signal: $H_\infty$ Nominal Controller (red) and Model Uncertainty (blue)

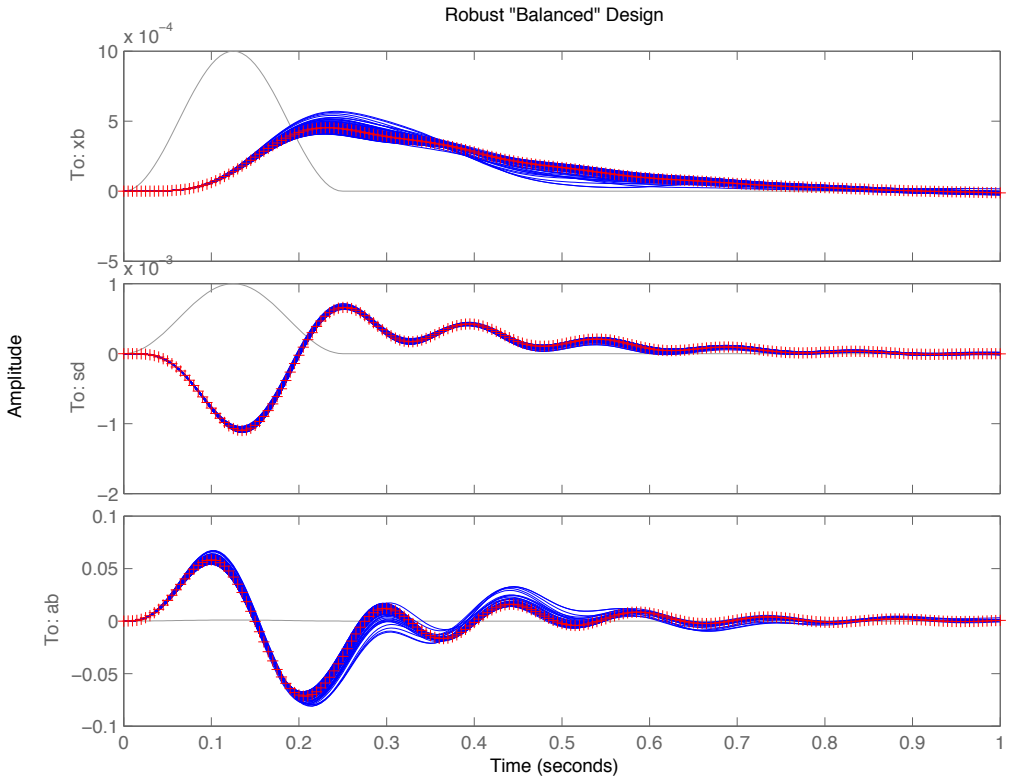



Figure 6.10: Time Response for Road Disturbance Signal: $\mu$ Synthesized Robust Controller (red) and Model Uncertainty (blue)

## 6.7 Other Papers/Other Control Methods

A paper by Li, Jing, and Karimi (2013) investigated output-feedback-based $H_\infty$ control for the quarter car suspension system with control delay. They showed that adding a control delay improved performance, especially achieving less body acceleration and further improvement for ride comfort [27]. Actuator delay also proved more effective in the presence of road disturbances. Therefore, they argue actuator delay is crucial in vehicle suspension. However, this may not be applicable to the Hyperloop. This system will need a very quick response and a control system with a fast time constant. A time delay may not be possible to implement.

LQG/LTR analysis was also emphasized in the literature for the quarter car suspension system (ElMadany & Abduljabbar, 1999 [16]), and similarly with the maglev system (Cai & Chen, 1996 [7]). This analysis was also implemented and results found were similar to what was seen in previous papers. They showed LQG/LTR was effective for this system. However, these results were not as interesting as the $H_\infty$ design so they were not included in this report.

## 6.8 Summary

$H_\infty$ controller synthesis with $\mu$ robustness design effectively balanced passenger comfort and handling for the quarter car model of the Hyperloop and was robust to model error and uncertainty. This control method was only applied to a simplified version of the Hyperloop suspension so it would be interesting to apply this control design to a more developed Hyperloop system model and compare the results found. In addition, the effect of control delay should be investigated first for the quarter car system and then considered for the Hyperloop's system. However, when considering the results of $H_\infty$ synthesis it should be noted that the resulting controller is only optimal for the cost function created. It may not be the optimal for performance measures typically used to evaluate controllers such as settling time, overshoot, or oscillatory behavior. There are many control methods and they may or may not end up with the same result. It is important to consider other methods and the potential benefits and drawbacks to using a different controller. In essence, effective control design is truly an art.

# Chapter 7

# Vacuum Pump Technology for the Hyperloop

## 7.1 Introduction

Vacuum pumps are essential to evacuate air from the Hyperloop tube before operation and to maintain tube pressure throughout the system's life. Vacuum pump stations will be built at regular intervals along the tube's length. Airlock chambers will be needed to transfer capsules from the open atmosphere to the vacuum and vice versa. This chapter analyzes the factors that affect tube pump-down times (vacuumizing the tube). The vacuumizing time affects the entire operation of the whole Hyperloop system. The factors that impact pumping times include orifice conductance, diameter of the tube, length of the tube, space between pumping stations, effective vacuumizing speed, and the target vacuum pressure. Based on desired properties available vacuum technologies were investigated and device suggestions were made.

## 7.2 Analysis for Tube Vacuumization Time

### 7.2.1 Orifice Conductance

An orifice links the vacuumizing pipe between the pump station and the Hyperloop tube. Flow resistance occurs as a result of external friction (gas molecules/wall

[7] Vacuum analysis adapted from [67]

surface) and internal friction (gas molecule/gas molecule, i.e. viscosity). The conductance will affect volume flow rate (pumping speed) of the vacuum. The orifice conductance can be calculated from the following formula,

$$C_0 = 3.36 \sqrt{\frac{T}{M}} A_0 \tag{7.2.1}$$

where $T$ is the ambient temperature (K), $M$ is the molar mass of the gass (g/mol), and $A_0$ is the orifice area ($cm^2$).

### 7.2.2 Long Pipe Conductance

For a round pipe, the pipe conductance is

$$C_1 = 3.81 \frac{D^3}{L} \sqrt{\frac{T}{M}} \tag{7.2.2}$$

where $D$ is the tube diameter (cm), $L$ is the tube section length (cm), and the other parameters are defined above.

Since the tube and the vacuumizing pipe are connected in series the equivalent conductance can be determined from a formula analogous to springs in series,

$$\frac{1}{C} = \frac{1}{C_0} + \frac{1}{C_1} \tag{7.2.3}$$

From vacuum theory the available vacuumizing speed can be determined from the following formula:

$$\frac{1}{S_e} = \frac{1}{S_0} + \frac{1}{C} \tag{7.2.4}$$

where $S_e$ is the available vacuumizing speed (L/s), $S_0$ is the nominal vacuumizing speed (L/s), and $C$ is the system conductance (L/s).

### 7.2.3 Vacuumizing Time

For a target tube pressure, $p$, tube volume, $V$, and available vacuumizing speed, $S_e$, the pump down time can be calculated from

$$t = \frac{V}{S_e} \ln \frac{p_0}{p} \tag{7.2.5}$$

Vacuumizing time is thus directly proportional to tube section volume and inversely proportional to available vacuumizing speed of the selected pump (see schematic in Figure 7.1).

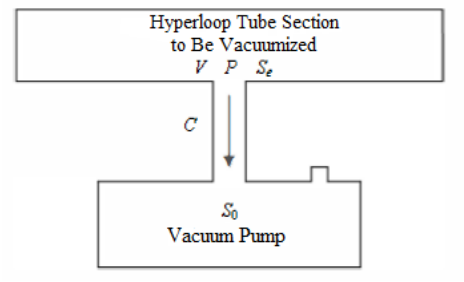



Figure 7.1: Schematic of Hyperloop tube section to be vacuumized

## 7.3 Numerical Analysis of the Vacuum Pump

### 7.3.1 Initial Pump-Down from Atmospheric Conditions to Target Tube Pressure

The orifice conductance ($C_0$) was computed using a typical orifice diameter ($D_0$) and other system parameters displayed in Table 7.1. The orifice conductance was found to be $C_0 = 3561$ L/s for this configuration.

| Vacuum Parameter | Value |
|---|---|
| $D_0$ (cm) | 20.0 |
| $A_0$ (cm$^2$) | 314.16 |
| $T$ (K) | 293.15 |
| $M$ (g/mol) | 29 |
| $C_0$ (L/s) | 3561 |

Table 7.1: Parameters for Determining Orifice Conductance

The effect of tube diameter and pump station interval distance on effective vacuumizing speed was examined. Tube diameter, $D$, was varied from 1.5 m to 5 m. The distance between the vacuum stations was used for tube section length, $L$, and this ranged from stations every 500 m to every 5000 m. For each combination of these values the conductance $C_1$ and $C$ were calculated as well as tube section volume, $V$. Assuming a nominal pump station vacuumizing speed of $S_0 = 1800$ L/s, the available

vacuuminzing speed was determined. The available vacuumizing speed was plotted using MATLAB as a function of tube diameter for various station intervals in Figure 7.2.

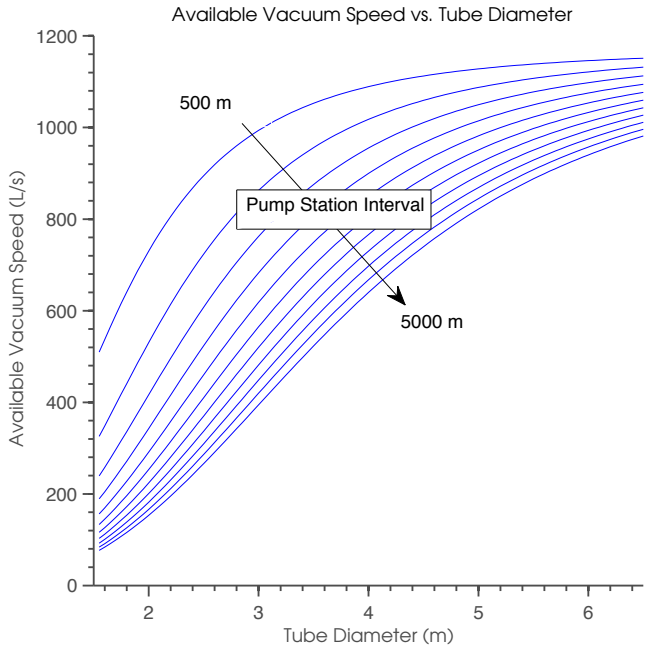



Figure 7.2: Available vacuumizing speed as a function of tube diameter for pump station interval distances from 500 m to 5000 m

The pump-down time was computed using Equation 7.2.5 for pump stations every 2 km; tube diameters 2.23 m (alpha), 3 m, 4 m, and 5 m; and available vacuumizing speeds, $S_e$, 200 L/s, 500 L/s, and 1000 L/s. The exponential dependence of pump-down time on target pressure can be observed in Figure 7.3. Lower target pressures will take longer to achieve and require more energy input to reach these levels. Since vacuumizing time directly depends on the square of the tube diameter, reducing the tube section diameter as far as possible will help shorten vacuumizing times and energy costs. Figure 7.4 takes a closer look at the pressures in the range of an operational Hyperloop (0-200 Pa). Starting at 200 Pa, the time only slowly increases until the target pressure is around 30 Pa. Upon reaching this point, the time begins to shoot up. Combined with the aerodynamic results seen in Chapter 3 that suggested only minimal drag reduction can be achieved by reducing the pressure past 40 Pa and the increased pumping times beyond this point, it is not recommended the tube pressure be less than 30-40 Pa for this vacuum pump configuration. Other vacuum configurations can be explored, but it becomes increasingly difficult to get higher vacuumizing times as the size and the complexities of these vacuum pumps increase.

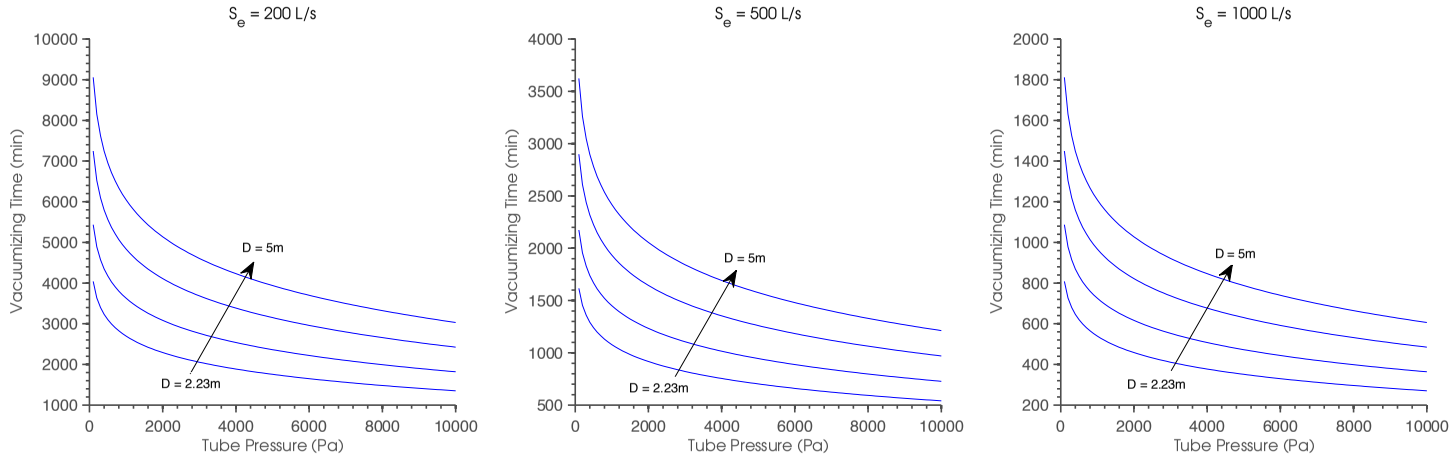



Figure 7.3: Vacuum pump-down time as a function of tube pressure for $D = 2.23$, 3, 4, and 5 m; $S_e = 200$, 500, and 1000 L/s

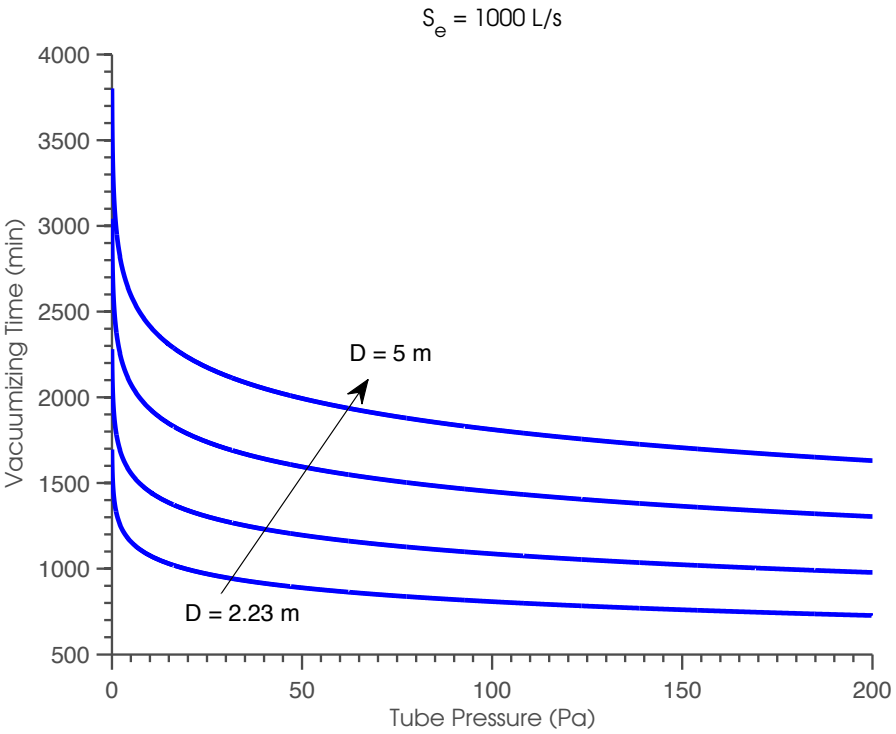



Figure 7.4: Vacuum pump-down time for tube pressures $P = 0$ - 200 Pa; tube diameters $D = 2.23$, 3, 4, and 5 m; available vacuumizing time $S_e = 1000$ L/s

### 7.3.2 Airlock Chamber Evacuation

There needs to be an interface between the atmospheric conditions of loading/unloading areas and the low pressure Hyperloop tube. An airlock chamber will be used and a vacuum pump will be needed to establish the appropriate pressure when capsules enter and exit the airlock. Equation 7.2.5 is again used to compute the times needed to establish the air lock pressure. It is assumed the airlock chamber has the same diameter as the Hyperloop tube, the length is 33 m (2 m longer than capsule's length to allow for clearance), the volume needed to be evacuated is equal to the volume of the airlock tube minus the volume of the capsule, and the nominal vacuumizing speeds range linearly from 1000 L/s to 12,000 L/s. Figure 7.5 reveals the same curve

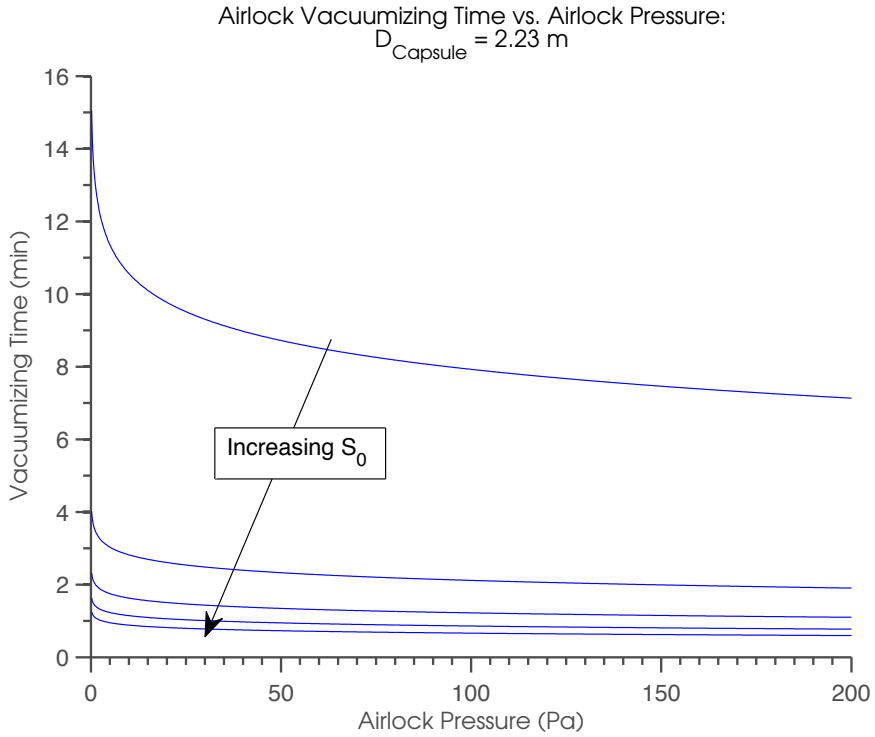



Figure 7.5: Airlock pump-down time as a function of target pressure for $D_{tube} = 2.23$ m and alpha document capsule size; Nominal vacuumizing speed ranges linearly from 1000 L/s to 12,000 L/s.

shape seen in the previous section. Furthermore, it can be seen that as nominal vacuumizing speed increases the curves begins to converge. This indicates it will be harder to achieve even faster pump-down times. The curves converge to around 40 s to 80 s airlock vacuumizing times for tube pressures of interest and $S_0$ ranging 8,000 L/s to 12,000 L/s. To indicate the difficulty of decreasing this time, to decrease the time in half the nominal vacuumizing speed, $S_0$, would need to be slightly more than

double (holding everything else constant). For example, to decrease pump-down time from 40 seconds to 20 seconds given a desired airlock pressure of 100 Pa, $S_0$ increases from 11,931 L/s to 23,954 L/s. This is a factor of 2.01 increase. Obviously, faster pump-down times will be desired in the airlock to make the trip length including loading/unloading minimal, but the costs of achieving faster and faster pump-down times begin to far exceed the benefits of faster times.

### 7.3.3 Power Requirements

The power requirements of the vacuum pump stations will contribute to overall system energy requirements. The average power requirements can be estimated using the following equation:

$$P = \frac{S_0 \, \Delta P}{\eta_{mech}} \tag{7.3.1}$$

A typical motor used for vacuum pumps will have a mechanical efficiency of $\eta_{mech} = 0.85$. Using the configuration examined in the previous subsections with $S_0 = 1800$ L/s and a target pressure of 100 Pa, Equation 7.3.1 yields an input power of 214.36 kW per pump for the initial pump down from atmospheric pressure.

## 7.4 Available Vacuum Pumps, Additional Influencing Factors, and Recommendations

When high flow rates (vacuumizing speeds) are required, a rotary vane backing pump can be combined with a Roots pump.

A rotary vane vacuum pump (Figure 7.6) is an oil-sealed rotary displacement pump. The electrically installed rotor (2) and the valves (3), which move radially under spring force, divide the working chamber into two separate spaces with variable volumes. As the rotor turns, gas flows into the enlarging suction chamber until it is sealed off by the second vane. The enclosed gas is compressed until the outlet valves opens against atmospheric pressure. Rotary vane pumps can be built in single- and two-stage versions.

Roots pumps (blowers) are a type of dry-running rotary displacement vacuum pump (Figure 7.7). They feature two synchronously counter-rotating rotors (4) in a figure-eight configuration separated by a narrow gap. One shaft is driven by a motor (1) while the other is synchronized by a pair of gears (6). Very high rotary speeds

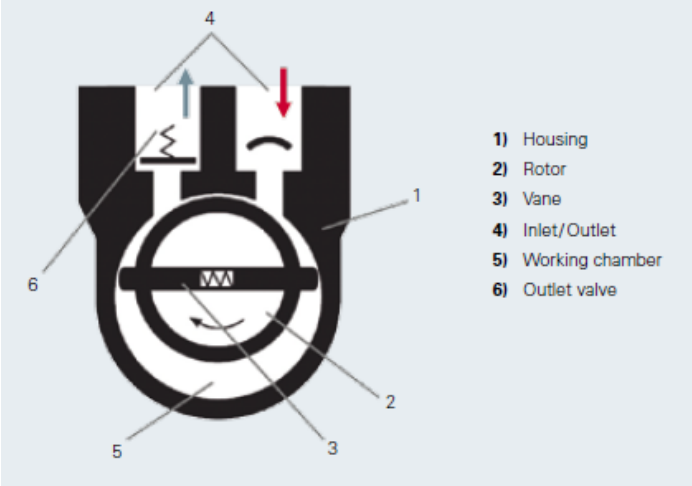



Figure 7.6: Rotary vane backing pump overview [41]

can be obtained because there is no friction in the suction chamber. Also, operational noises are very low due to the absence of reciprocating masses. One downside of roots pumps arises from the high level of energy dissipation generated in the presence of high pressure differentials. This places a limit on the pressure differential. Roots pumps cannot discharge against atmosphere because they cannot compress the air fast enough and, therefore, require a backing pump.

According to Pfieffer Vacuum a rotary vane vacuum pump is the most cost-effective backing pump for a roots vacuum pumping station [41]. Even at atmospheric pressure, a Roots vacuum pump with overflow valves can be switched on together with the backing pump. This increases the pumping speed right from the start and shortens evacuation times. While the rotary pump does almost all the work at the start, as the inlet pressure decreases the Roots pump kicks in and boosts the pumping speed of the backing pump. This extends the ultimate pressure of the system. Water vapor and other solvent vapors can be extracted using this setup.

Several technical challenges arise with vacuum pumps in this pressure range. The vacuum pump selected will have an ultimate pressure below the desired tube pressure if the pump is left running. A control mechanism such as a leaking valve, bleeding mechanism, or mass flow controller will be needed in combination with precise pressure gauges. Simply turning the pump off when the desired pressure is reached and then back on when a large enough deviation has occurred may be very inefficient. Power requirements are very high for start up of vacuum pumps, but they become much lower once in operation. Thus, further investigation is required to see what type of control scheme is needed to deal with pressure changes in the Hyperloop tube. In

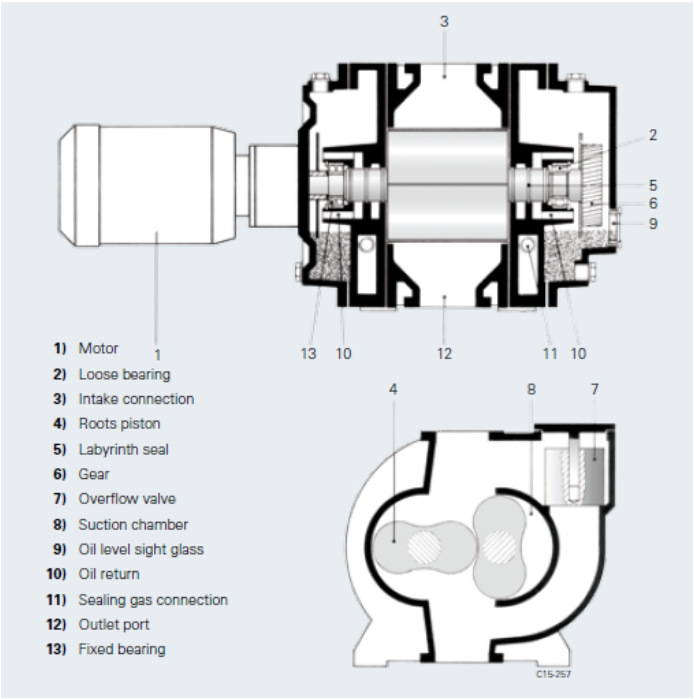



Figure 7.7: Roots vacuum pump overview [41]

addition, leaks and the permeation of materials can be harmful if not designed properly. During the first pump-down of the tube, the pump is dealing with ambient air. There are approximately 10 grams of water vapor per $m^3$ so water vapor will always be present on all surfaces to start. Other contaminants such as oil and grease from screws and seals should be avoided. The associated outgassing effects can increase pump-down times due to water and grease evaporating off. Also, air molecules will be trapped in bolt threads and they can slowly leak into the tube chamber. To avoid this problem special bolts are designed with slits to allow air to escape. When determining the number of pumping stations to put along the Hyperloop track, the fact that pumps are mechanical devices and need servicing should be taken under consideration. Backing pumps will occasionally be taken offline to change oil as well as deal with any other mechanical issues in the pumping system. It is essential to account for the time a pump is offline. If the pumping station interval distance is short or there are many pumps per station, the conditions inside Hyperloop system will not be as heavily impacted by a single pump going offline as if there were less pumps supporting the system. Having more pump stations will also allow for more efficient leak detection and solving. Therefore, vacuum pump redundancy is essential.

A pump configuration similar to the Pfieffer's CombiLine WU 1902 would be recommended for the Hyperloop because it is single-stage rotary vane pump combined

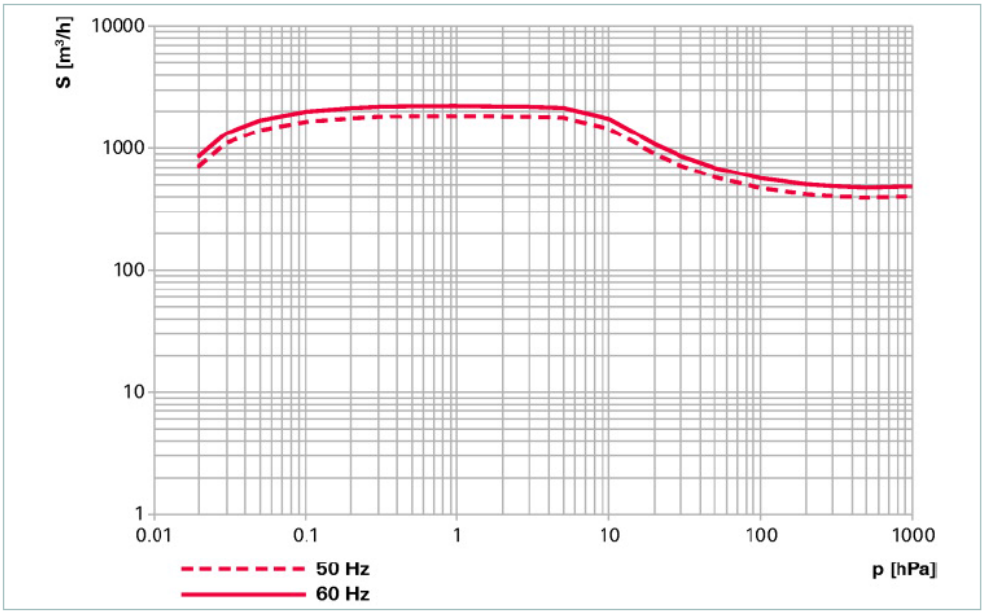



Figure 7.8: Pfieffer CombiLine 1902 - Roots pump with single-stage rotary vane pump: Pumping speeds as function of pressure [40]

with a Roots pump. The pumping speed characteristics can be observed in Figure 7.8 and it is evident the pumping speed is lower when the pump initially begins with atmospheric conditions. The available vacuumizing speed then increases once the tube pressure hits 100 hPa (1000 Pa) as the Roots pump has fully kicked in and provides extra boost to pumping speed. The maximum pumping speed is 2200 $m^3$/h (611 L/s) and the ultimate pressure ranges from 0.3 Pa to 0.08 Pa. The power spec is around 22 kW with 230 V or 460 V options for the three phase motor [40]. Using Equation 7.3.1 with $S_0$ = 2200 $m^3$/hr and target pressure of 100 Pa yields a power of 72.8 kW, more than three times the observed value. Thus, Equation 7.3.1 may not be the best for estimating the power required for a Roots pump backed with a single-stage rotary vane pump. In addition, the power input to the drive motor will change as intake pressure reduces. While the data was not available for this unit, the behavior will be similar to the motor supply to Oerlikon Leybold Vacuum's rotary plunger pump in Figure 7.9 despite the pumping speed being much less ($S_e$ = 60 $m^3$/hr)[36].

Although the Pfieffer CombiLine WU 1902 has a slightly lower pumping speeds than desired for the Hyperloop, especially for the airlock vacuumizing, it is the largest commercially sold of its type with a price tag. A representative from Pfieffer discussed larger pumps with faster pumping speeds can be designed and sold, but prices will

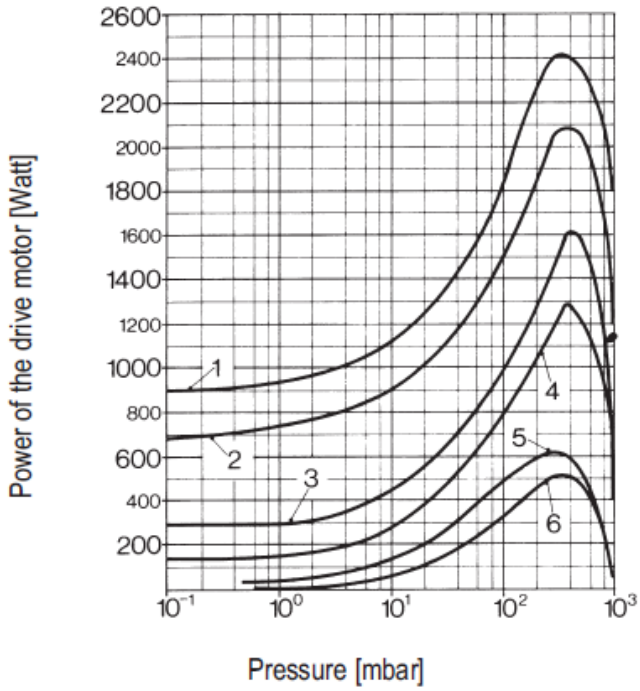



Figure 7.9: Rotary plunger pump ($S_e$ = 60 m$^3$/hr) motor power as a function of intake pressure an operating temperature [36]. Other pumps will have similar power behavior.

vary for custom projects. The Combiline WU 1902 will cost $23,900 for a single unit and $17,000 for mass order. The vacuum company recently sold a single unit of a Roots pump backed with a single-stage rotary vane pump with pumping capabilities of 27,000 m$^3$/hr (7500 L/s) for $250,000. While this high magnitude of pumping speed may not be needed for initial pump-down, this pumping station would be more ideal for the Hyperloop airlock interface. The maximum nominal vacuumizing speed seen in these type of pumps is 12,000 L/s [67]. The ultimate pressure of Pfieffer CombiLine WU 1902 pump station is lower than needed for Hyperloop operation. In part, this is necessary because a degree of oversize is required for initial pump down. Yet, as indicated earlier, when a pumping station has a lower ultimate pressure than desired a control mechanism will be necessary. A further factor to consider is that these pumps cannot be left outside and exposed to rain, snow, etc. The temperature limits for a station like the Pfieffer CombiLine is $12 - 40\,^{\circ}$C. This is a reasonable temperature range for an area like Southern California, but further studies are required to establish

what happens when it gets too hot or cold, and if an air conditioned room with heating capabilities for the winter is necessary.

## 7.5 Summary

This chapter revealed that vacuum pump-down time goes as the square of the diameter, and thus the smaller the tube the faster the target pressure can be achieved. In addition, higher vacuumizing speeds shorten the pump-down time, but vacuum pump stations become more complex and expensive to build/operate as higher pumping speeds are demanded. The interval distance between pumping stations is very important as pump-down time is directly proportional to this distance. The shorter the interval, the faster the times. A balance needs to be achieved between the amount of pumping station infrastructure, pumping times, and effect of station servicing. A suggested interval distance is 2 km between pumping stations. The desired degree of vacuum in the Hyperloop is the most important factor as vacuumizing time increases exponentially as target pressure decreases. In combination with the results of aerodynamic drag and pressure it is suggested tube pressure not be reduced below 40 Pa. For the alpha document conditions with a target tube pressure of 100 Pa, pumping stations every 2 km, and a vacuum pumping station similar to the Pfieffer CombiLine WU 1902 Roots pump with rotary vane backing pump ($S_e$ = 500 L/s), the pump-down time for each tube section would be 1616 minutes or nearly 27 hours. There is the possibility to decrease this time with custom designed and built vacuum stations with higher pumping speeds. It is highly recommended for the airlock chambers to design a custom pumping station with at least $S_0$ = 8000 L/s in order to keep the vacuumizing time less than 1 minute.

# Chapter 8

# Hyperloop Compressor

## 8.1 Introduction

A factor limiting the high speed movement of the Hyperloop capsule through a tube containing air is the Kantrowitz limit. For a given tube to capsule ratio there is a maximum speed that will choke the flow. If the capsule is too close to the tube's walls then the capsule will eventually be forced to push the entire column of air in the system. The Kantrowitz limit constrains the system to either go slowly or have a very large tube diameter, neither of which are ideal. The proposed solution is to mount an electric compressor fan on the nose of the pod that will actively transfer high pressure air from the front to the rear of the capsule. Throughout the journey the weight of the capsule will be supported by an air bearing system and this compressor will also serve to supply the necessary air.

## 8.2 Alpha Compressor Design

The processing of air through the alpha compressor design can be seen in Figure 8.1. Using energy balance, mass and momentum conservation, and isentropic approximations this system can be analyzed. It was first discovered that by using the alpha design, the incoming flow to the first axial compressor is too fast and turbulence will cause the flow to become supersonic locally. It is very expensive to operate a compressor when shock waves are forming inside so a diffuser is needed to slow the flow down before the air is compressed. This was corroborated by a preliminary CFD analysis the company ANSYS ran on the proposed Hyperloop capsule design.

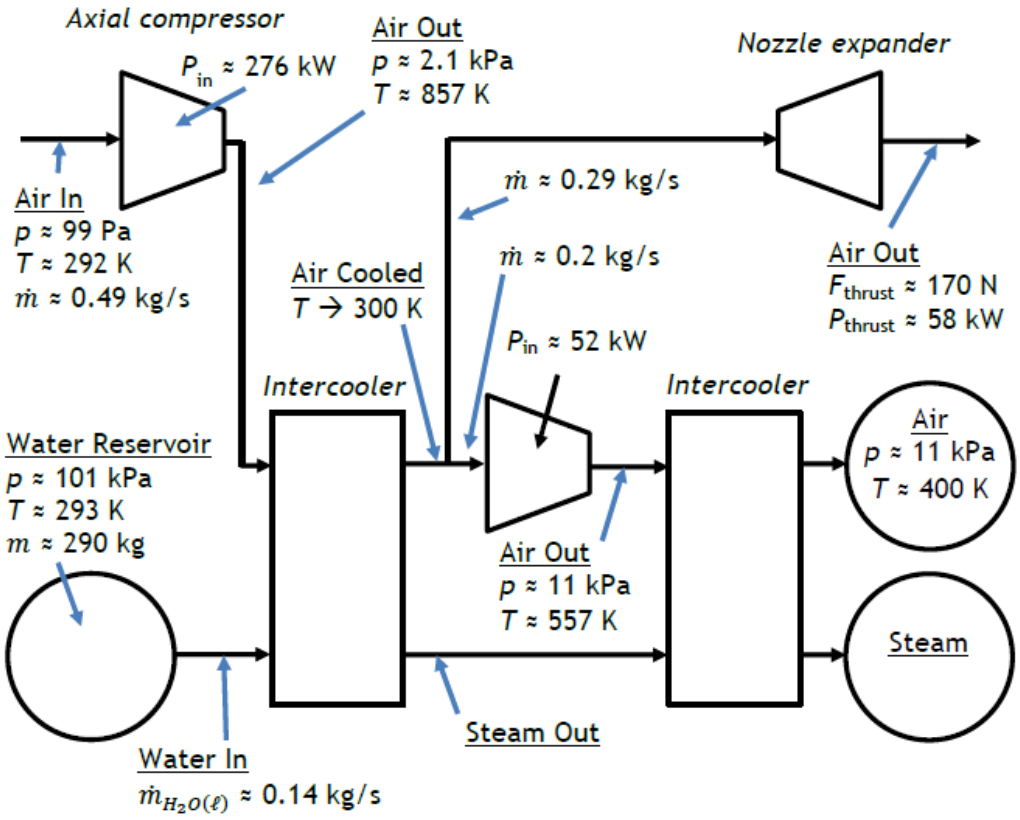



Figure 8.1: Alpha Compressor Schematic [34].

## 8.3 Diffuser Compressor Design

Stagnation properties will be used for the analysis of a design with a diffuser in front of the axial compressor. Assuming compressible flow through the diffuser and constant specific heats the outlet pressure to the diffuser is

$$p_{02} = p_{tube}\left(1 + \eta_d \frac{\gamma - 1}{2} M^2\right)^{\frac{\gamma}{\gamma - 1}} \tag{8.3.1}$$

where $\eta_d$ is the diffuser efficiency (98%), $M$ is the Mach number of the incoming flow, and $\gamma$ is the ratio of specific heats. Because the diffuser will be adiabatic, the stagnation outlet temperature is

$$T_{02} = T_{tube}\left(1 + \frac{\gamma - 1}{2} M^2\right) \tag{8.3.2}$$

Using the alpha tube conditions for the maximum capsule speed ($u_{e,\,max}$), $p_{02} = 184.95$ Pa and $T_{02} = 350.6$ K.

The mass flow rate of air through the compressor is limited by the capsule speed, tube air density, and inlet area. The density of the air in the evacuated tube is very low so there are less air particles available to the compressor. The maximum reasonable inlet area is assumed to be 87% of the capsule's frontal surface area. For a tube pressure of 100 Pa and maximum capsule speed ($u_{e,\,max}$), the maximum mass flow rate through the compressor ($\dot{m}_c$) is about 0.49 kg/s. The pressure ratio of the compressor can be found from the compression ratio ($r_p = r^\gamma$). The alpha design compression ratio, $r = 20$ will be used at first. The outlet pressure from the axial compressor is then

$$p_{03} = r_p\, p_{02} \tag{8.3.3}$$

and the outlet temperature is

$$T_{03} = T_{02}\left[1 + \frac{1}{\eta_c}\left(r_p^{\frac{\gamma-1}{\gamma}} - 1\right)\right] \tag{8.3.4}$$

where $\eta_c$ is the isentropic efficiency of the compressor (85%). The power input is given by

$$P_{motor} = \dot{m}_c\, c_p \frac{T_{02}}{\eta_c}\left(r_p^{\frac{\gamma-1}{\gamma}} - 1\right) \tag{8.3.5}$$

Using the alpha parameters, it is found that $p_{03} = 12.26$ kPa, $T_{03} = 1305$ K, and $P_{motor} = 470$ kW. This configuration requires more power input and achieves a much higher pressure than needed and a hotter temperature than desired. It is therefore suggested that the compression ratio be lower than 20, especially since having the diffuser raises the inlet pressure to the compressor. A compression ratio of 9 gives a static compressor outlet pressure of $p_3 = 2.14$ kPa and a static temperature $T_3 = 779$ K, which are very close to the values listed in the alpha design. This lowers the power input to 286 kW. Using mass conservation and assuming the area ratio of the compressor outlet to inlet is 0.7, the exit velocity of the compressed air is 60.23 m/s.

After the first axial compressor, the air is cooled and about 60% of this air is bypassed via a narrow tube near the bottom of the capsule to the capsule's tail. The nozzle expands the flow, generating thrust to make up for the losses due to the aerodynamic drag. The remainder of the cooled air travels to a second compressor where the air is compressed to the pressure desired for the air suspension system. This air is then again cooled via an intercooler and then stored in an onboard pressure

vessel until it is needed by the air suspension system.

Assuming the static temperature is 300 K after running through the the first intercooler and the mass flow rate going to the second compressor is 0.2 kg/s, the power input needed for the second compressor to bring the static output pressure to 11 kPa is 42.5 kW. The compression ratio required is 3.3 (lower than the 5.1 suggested by the alpha document) and the static output temperature is 510.5 K. The alpha document estimates 1500 kg worth of batteries can provide 45 minutes of onbaord compressor power. These batteries can then be changed and each stop where they will be recharged. The second intercooler will then reduce the temperature of this compressed air to 400 K for storage in a pressure vessel above the air suspension system.

## 8.4 Intercoolers: Water Coolant Mass Flow Rate

The amount of water needed to cool the air at the two intercooolers was investigated. Using the alpha document values for the water reservoir in Figure 8.1, the mass flow rate of water needed to cool the compressed air to the desired levels using both intercoolers was computed.

It is assumed the intercoolers achieve constant pressure cooling. Taking a look at the first intercooler, the heat absorbed can be found from

$$\dot{Q}_{absorbed} = \dot{m}_{H_2O,\,(l)}\, c_{p,\,H_2O}\, (T_{out,\,H_2O} - T_{in,\,H_2O}) \tag{8.4.1}$$

which is equal to the heat released by the intercooler

$$\dot{Q}_{released} = \dot{m}_{air}\, c_{p,\,air}\, (T_{comp2,\,in} - T_{comp1,\,out}) \tag{8.4.2}$$

where $T_{comp1,\,out} = T_3$, $T_{comp2,in} = 300$ K, $T_{in,\,H_2O} = 293$ K, and $T_{out,\,H_2O}$ will be determined by examining the second intercooler. The specific heats at constant pressure for liquid water and air are $c_{p,\,H_2O}$ and $c_{p,\,air}$, respectively. The mass flow rate of air is the mass flow rate of air through the first compressor (0.49 kg/s). The mass flow rate of the liquid water is unknown and will be solved for. Similar equations can be established for the second intercooler using only the air mass flow rate though the second intercooler (0.2 kg/s). The known parameters for the second intercooler are the inlet and outlet temperatures of the air, which are, respectively, the outlet temperature from the second compressor ($T_5 = 510.5$ K) and the desired temperature of

the pressure vessel air ($T_{vessel} = 400$ K). The output water temperature of the second intercooler is assumed to be the temperature that will just make the phase transition to steam (373 K). The inlet water temperature is equal to the outlet temperature of the water from the first intercooler. This will then produce a system of two equations with two unknowns ($\dot{m}_{H_2O,(l)}$ and $T_{out,H_2O}$).

It was found that a much larger mass flow rate of water was needed than anticipated by the alpha document. The $\dot{m}_{H_2O}$ was computed to be 0.77 kg/s compared to the alpha document's 0.14 kg/s (typical mass flow rate for intercoolers found in racing cars). This is significant because the mass flow rate dictates the mass of water each capsule will need to carry onboard. Assuming a total trip time of 35 minutes, the mass of water needed to be stored would be 1617 kg (compared to 294 kg for the alpha document). This mass increase (also container volume increase) is significant and the effects will propagate throughout the rest of the design. For example, more compressed air input will be needed for the air suspension system in order to maintain capsule levitation. This will mean the compressors will need to raise the pressure slightly higher. This will correspond to more energy input as well as a higher output temperature from the compressors. The higher output temperatures will then need even more water to cool to the desired temperatures, increasing the onboard water mass further. Iterations on these calculations will need to be run when implementing a full design.

Upon closer inspection, the mass flow of liquid water presented in the alpha document can be achieved if the temperature of the steam is allowed to be higher. A water mass flow rate of 0.14 kg/s will be required if the temperature of the steam is 730 K. Further investigation is needed to determine if this higher temperature of steam would be a problem. In addition, the possibility of not cooling the bypassed air to the capsule tail should be explored. If this air is not cooled, then less air needs to be cooled and less mass of water coolant is required.

The steam reservoir needs some more attention than given in the alpha document. The volume requirements of the steam reservoir will be much larger than those of the water reservoir because steam has a much lower density. The enthalpy of steam is also much higher, and if the steam is needed to be compressed before storage this will require additional energy input. The alpha document suggested the steam reservoir will be swapped out after the journey, but provided no volume specifications. There may be a better method for a heat sink than using water. Certain metals will be more effective, but at the cost of larger mass. These alternative heat sinks should be explored.

## 8.5 Summary

The primary purpose of the compressor is to prevent the flow from choking. In addition, the compressor will supply high pressure air to the air suspension system as well as provide some additional thrust at the rear of the capsule. A major adjustment to the alpha compressor design was found to be adding a diffuser in front of the first compressor. This will help prevent the air from going supersonic locally at the compressor. In addition, this would also compress the air before the inlet to the compressor, lowering the required compression ratio and motor input power required. Many assumptions made by the alpha design were used in the evaluation of this design. Many of these parameters could be optimized based on the analysis of the other subsystems. For example, the amount of air bypassed to the tail of the capsule and the amount routed to the air suspension system should be investigated. The amount of air required by the air suspension system will be the driving factor. It was found that at the low pressure of the tube that the aerodynamic drag is not large enough to significantly slow the capsule so the amount of thrust gained back from the nozzle should only be considered as a bonus, not a major design parameter. Preventing the airflow from going supersonic will put a limit on this thrust generated. It is recommended that this be investigated in future designs. The heat released by the capsule compressing air, then expelling it downward and backward has raised concern from many critics. It appears the water cooling system will need to have a larger flow rate than originally anticipated, but further research is needed.

# Chapter 9

# Modeling the Hyperloop Route

## 9.1 Introduction

The proposed alpha route from Los Angeles to San Francisco will maintain a path as close as possible to the established right-of-way while respecting existing structures to reduce capital costs. This route will follow I-5 and I-580 for the majority of the 563 km journey with the tube construction in the median. There exists the possibility to have more stations and split tracks along the way, but these will not be considered at this time. The capsule will carry 28 passengers and depart on average every two minutes according to the alpha document. To ensure passenger comfort, lateral acceleration is limited to $0.5g$ and longitudinal acceleration is limited to $1g$ during propulsion. Propulsion stations will be optimized to ensure appropriate $g$-force is experienced by passengers and to maintain speed. The absolute max speed is limited by the condition by which the flow will become sonic and form shock waves (assumed to $M = 0.99$). The other constraint on the capsule's speed is imparted by the bend radius of the route so passengers do not experience lateral accelerations greater than $0.5g$. In some places the route will need to be altered from the highway in order to mitigate $g$-force concerns. Different sized pylons and tunneling will also be used to minimize elevation changes.

This chapter looks into the Hyperloop route focusing on the capsule's speed and position over the trip length, as well as overall trip time. The route path is modeled for the propulsion stations that will keep $g$-forces at a comfortable level and using the aerodynamic drag force derived in Chapter 3 to get the system's dynamics.

## 9.2 Route Visualization

### 9.2.1 Capsule Deceleration

The capsule's deceleration was examined in the absence of the reboost propulsion stations for the three cruising speeds using the aerodynamic force model from Chapter 3 and solving the differential equation established by Newton's second law

$$\ddot{x} = \frac{F_{tot}}{m_c} \tag{9.2.1}$$

where $F_{tot}$ is the total aerodynamic drag force, and $m_c$ is the capsule's total mass. This differential equation is solved to find the capsule's position and velocity as functions of time (Figure 9.1 and Figure 9.2 respectively) due to the aerodynamic drag forces (Figure 9.3) acting on the body. The power loss (kW) due to the aerodynamic drag forces is plotted in Figure 9.4 and ranges from 18 to 260 kW.

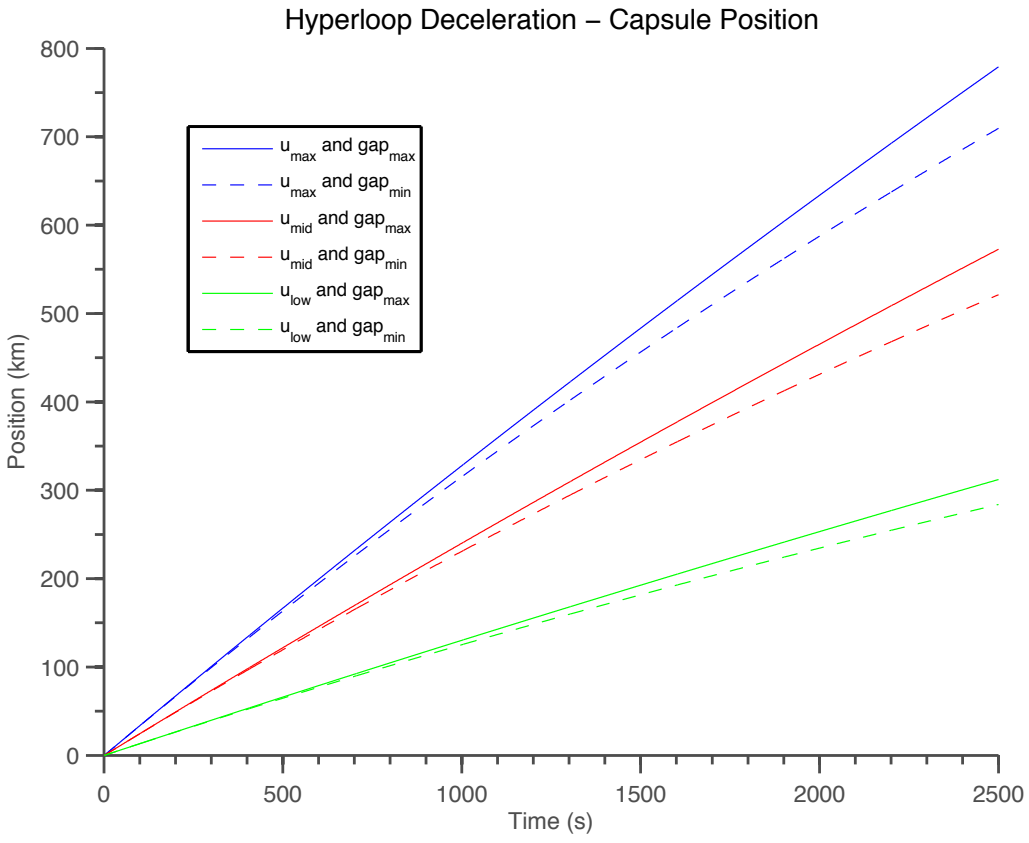



Figure 9.1: Position of Hyperloop capsule as it decelerates due to aerodynamic drag.

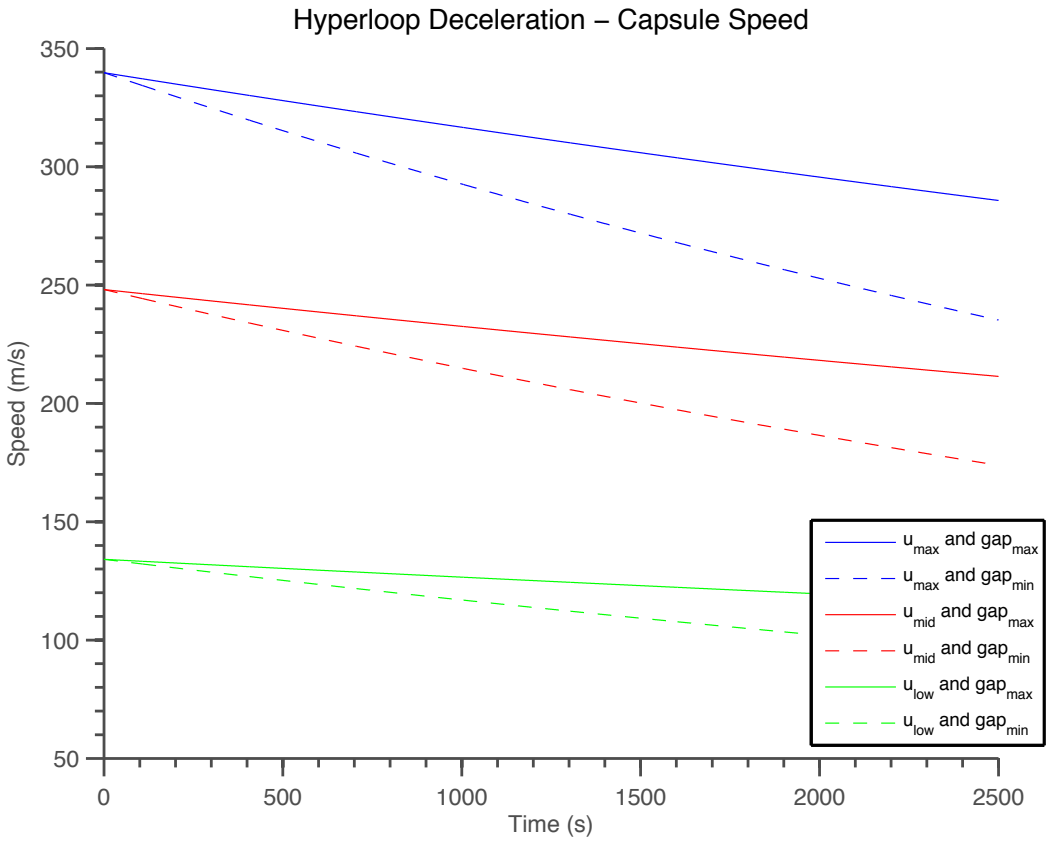



Figure 9.2: Speed of Hyperloop capsule as it decelerates due to aerodynamic drag.

### 9.2.2 Preliminary Bend Radii Analysis

Throughout the Hyperloop's journey the path will need to turn. To ensure passenger comfort, turns will need to be taken at a maximum of $0.5g$ of lateral acceleration. There is the possibility of banking the capsule in the tube during turns, but it is assumed this type of system is not in place for this analysis. Table 9.1 contains the minimum bend radius for turns at each of the three cruising speeds ($u_{e,\,max}$ , $u_{e,\,mid}$ , and $u_{e,\,low}$) using Equation (9.2.2). These results confirm the suggestions found in the alpha document.

$$r_{min} = \frac{u_e^2}{0.5g} \tag{9.2.2}$$

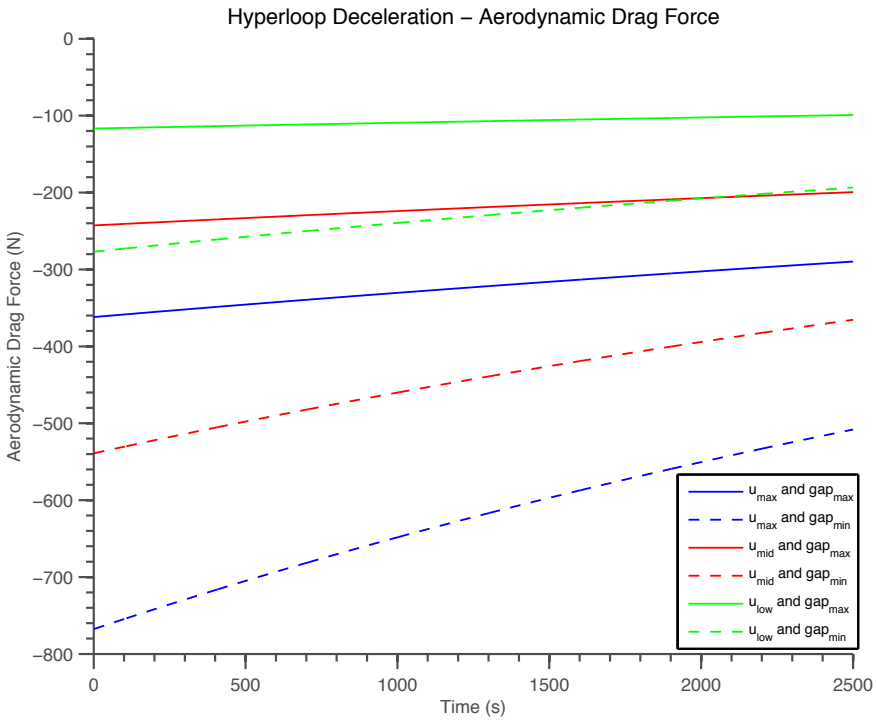



Figure 9.3: Aerodynamic drag force acting on Hyperloop capsule as it decelerates.

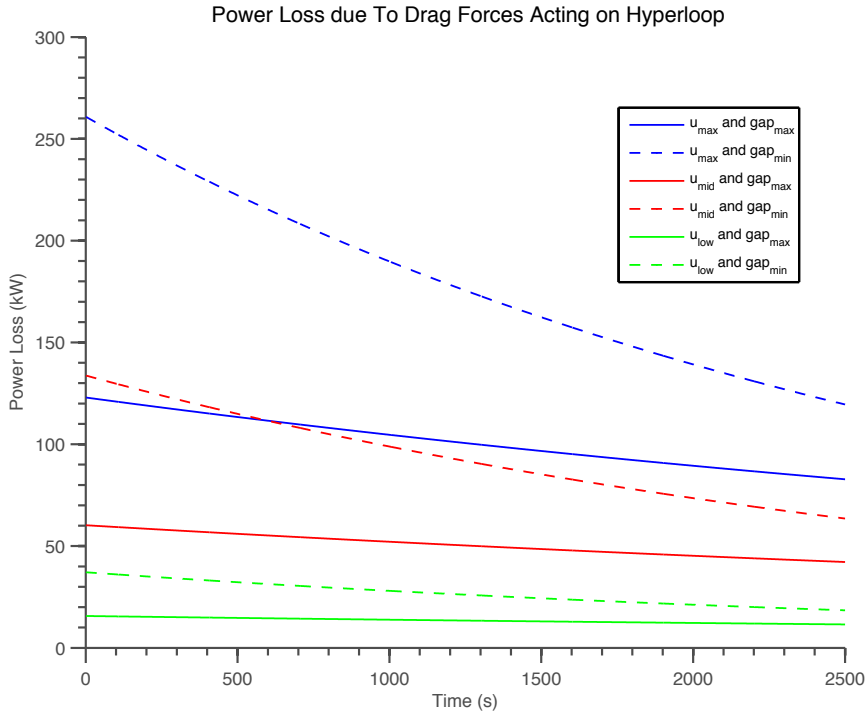



Figure 9.4: Power loss due to aerodynamic drag force acting on Hyperloop capsule as it decelerates.

Table 9.1: Minimum bend radius for $0.5g$ lateral acceleration.

| Capsule Speed (m/s) | Min Bend Radius (km) |
|---|---|
| $u_{low} = 134.11$ | 3.67 |
| $u_{mid} = 248.11$ | 12.6 |
| $u_{max} = 339.75$ | 23.5 |

### 9.2.3 Route Journey: Speed and Position as Functions of Time since Departure

The route considered features three propulsion stations to accelerate the vehicle after leaving Los Angeles and three propulsion/regenerative braking stations to decelerate the vehicle before arriving in San Francisco. Undoubtedly, top speed should be reached as soon as possible and maintained for as long as possible to minimize total trip time. However, the track path puts limitations on the vehicle speed for certain sections of the track. If the route is to follow the interstate system and respect existing structures, the bend radius of the track will be much smaller at the start and end of the journey as the roadway makes many turns through the suburbs. The defined bend radius of the roadway and the condition of $0.5g$ lateral acceleration puts a constraint on the capsule speed. The middle section features right-of-way which is much straighter, and thus faster speeds can be reached. The alpha document lists the distances along the route that need to be traveled at the low speed, at the mid speed, and at the high speed. In addition, it lists the times after departing L.A. when the capsule reaches a propulsion/braking station (Table 9.2).

Table 9.2: Alpha route segment times and distances traveled since leaving L.A.

| Track Segment | $\alpha$ time(s) | $\alpha$ distance traveled(km) |
|---|---|---|
| $u_{low}$ Depart. | 0 | 0 |
| $u_{mid}$ Depart. | 167 | 21.60 |
| $u_{max}$ Depart. | 435 | 86.00 |
| $u_{max}$ Arriv. | 1518 | 480.75 |
| $u_{mid}$ Arriv. | 1618 | 503.06 |
| $u_{low}$ Arriv. | 2134 | 563.00 |

First, the suggested alpha section times for the route are used to evaluate the aerodynamic drag force model used by the alpha document staff compared to the model developed in Chapter 3. A plot of the capsule's position as a function of time since departure from L.A. will reveal if the capsule will actually arrive in San Francisco using these suggested propulsion times. Then, using the alpha section distances corresponding to each speed the Chapter 3 aerodynamic analysis will be used to carry out the journey to completion with an arrival in San Francisco. Figures 9.5 and 9.6 show the speed and position plots as functions of time since departure in L.A. From this analysis it was found that using the alpha document timing recommendations the capsule would not actually reach San Francisco. The final position for this analysis is only 534.8 km compared to the total trip distance of 563 km stated in the alpha document. Optimizing the journey for the given speed sections lengths, the journey is visualized to completion. The differences between the blue (alpha times) and red (required alpha section lengths) reveal that the alpha times do not allow the capsule to coast at maximum speed for long enough, and thus the capsule would not reach San Francisco under these conditions. The total time to get from L.A. to San Francisco using the alpha segment distances and the aerodynamic drag model from Chapter 3 is 2181 seconds (36.35 min). This is 47 seconds longer than the total time proposed in the alpha document (2134 seconds). Compared to the Califronia High Speed Rail trip time of 2 hours 38 minutes, the time saved is huge.

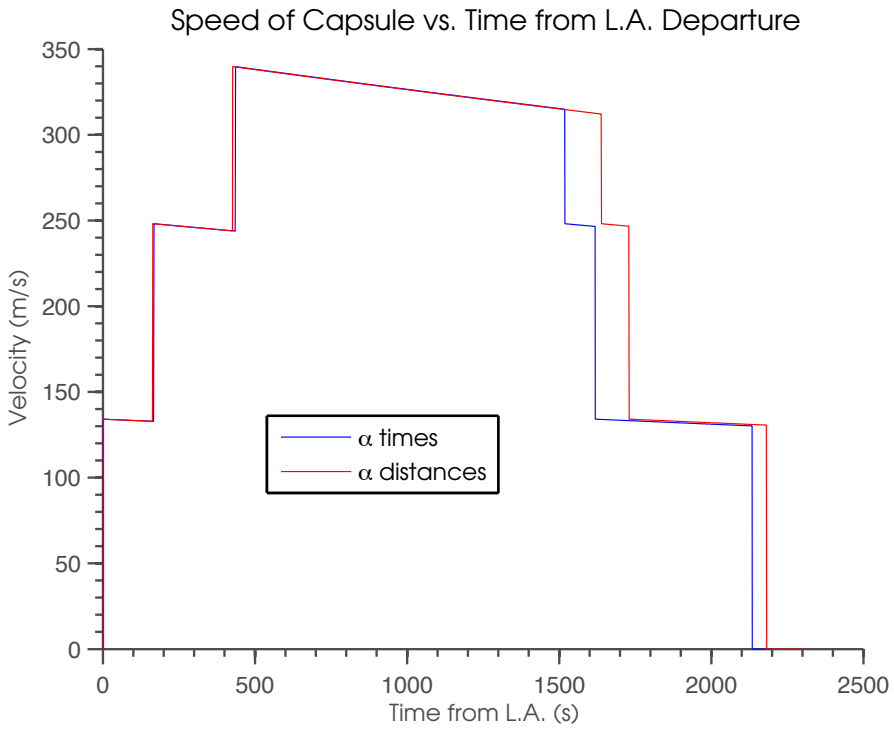



Figure 9.5: Speed of Hyperloop capsule as a function of time from L.A. departure.

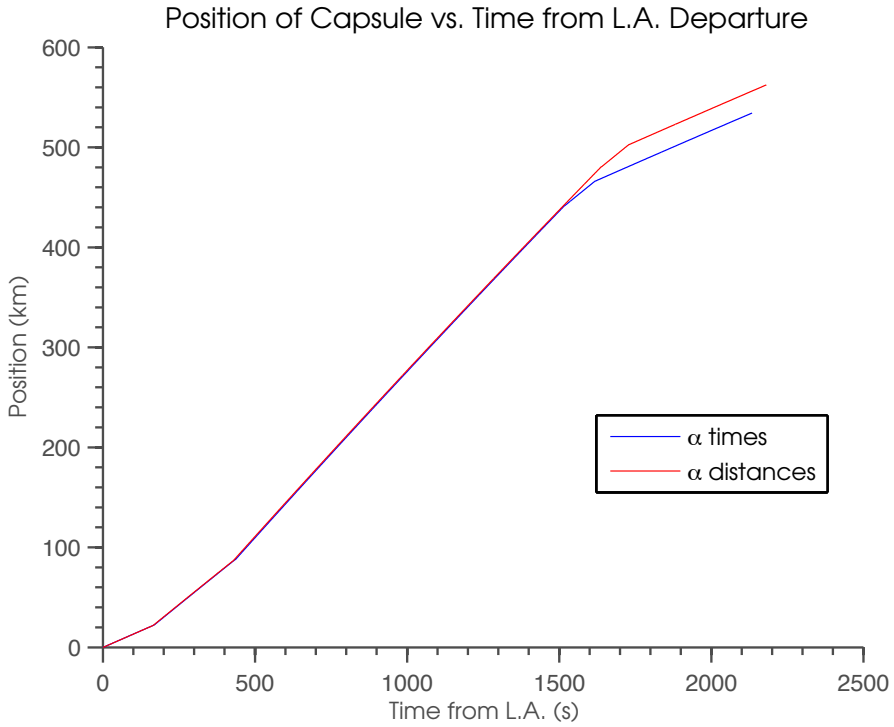



Figure 9.6: Position of Hyperloop capsule as a function of time from L.A. departure.

### 9.2.4 Departure Separation, Passengers, and Number of Capsules

During peak business hours the Hyperloop will want to maximize the number of passengers transported. The minimum departure delay between two capsules will ensure there is never a collision and is calculated under the assumption that the the trailing capsule can stop as soon as there is an emergency with the leading capsule. The minimum departure delay for $1g$ deceleration is about 27 seconds. The minimum acceleration needed to stop under a range of departure delays is compiled in Table 9.3. Figure 9.7 plots the distance between two capsules as a function of time since departing L.A. for these same departure delay times. The minimum deceleration curves are overlaid on these plots (dotted red lines) to show what segments in the journey impose these minimum deceleration for each departure delay time. The regions where each blue curve and its corresponding minimum deceleration red curve almost intersect is circled in green. It can be seen this only happens in the first two segments of the journey. Once the first capsule gets to full speed, it is much more difficult for the second capsule to ever catch up.

Table 9.3: Departure delays and minimum deceleration rates

| Departure Delay (s) | Minimum Deceleration |
|---|---|
| 27 | $1g$ |
| 60 | $0.420g$ |
| 90 | $0.275g$ |
| 180 | $0.135g$ |
| 300 | $0.085g$ |

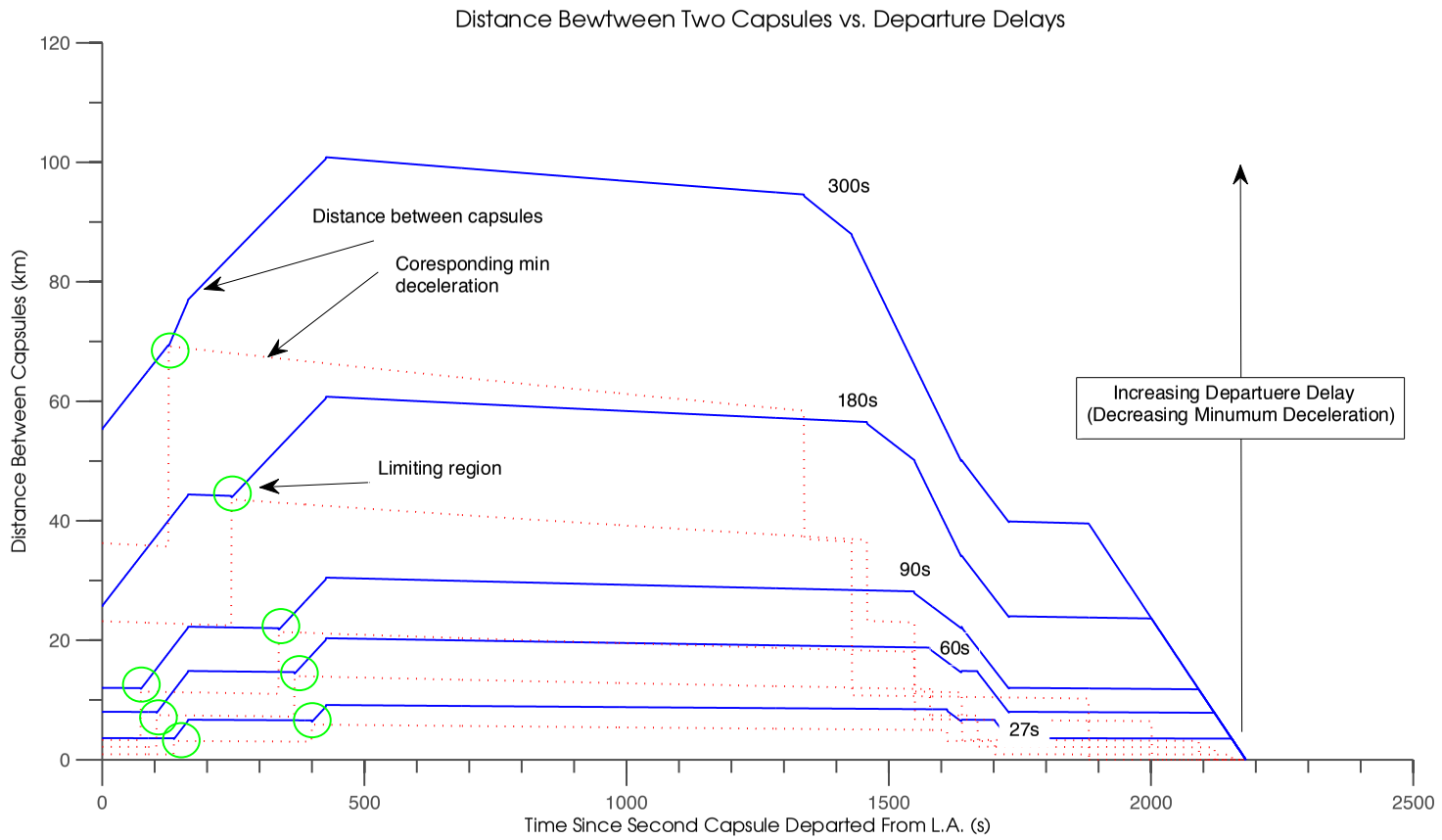



Figure 9.7: Distance between two capsules as a function of time since the second capsule departed L.A. plotted for multiple departure delay times. Minimum deceleration is overlaid (dotted red curve) to indicate regions where close contact would occur (green circled areas).

The number of Hyperloop passengers per hour is plotted as function of time in Figure 9.8 for different sized capsules (20, 28, and 40 passengers). For the 28 person capsules and a 30 second departure delay, the Hyperloop can transport 3,733 passengers per hour each direction. To compare to other modes of transportation, a freeway lane can carry 2,000 cars per hour, the California High Speed Rail has a capacity of 12,000 passengers per hour, and subways running at a 3 minute headway can carry 36,000 passengers per hour [58] [8]. While these modes may have larger capacities, they rarely fill to capacity. In addition, these modes take longer to reach the same final destination, thus using the Hyperloop more people will actually reach the final destination for the same amount of time.

The number of operational capsules is an important factor when constructing the Hyperloop. It is assumed there will need to be 3 spare capsules when maintenance issues arise. The number of capsules then depends on the delay time between capsule departures and the amount of time needed to prep and load a vehicle. The number computed is multiplied by two since the track goes in both directions. This is also plotted in Figure 9.9. For load times 1 to 10 minutes and a departure delay of 30 seconds the number of capsules ranges from 155 to 191. This is substantially more than the 40 capsules proposed by the alpha document. In order to only need to have 40 capsules the average departure delay for these load times would range from 132 to 164 seconds, which is larger than the discussed average departure time of 2 minutes. The configuration that best balances maximizing passengers transported and minimizing number of capsules required is for a departure delay of 50 seconds, corresponding to 2,016 passengers transported per hour and 105 capsules required (5 minute load time and 28 passengers per capsule). However, 30 second departure delay times may be needed in peak hours and if capsule cost is not a large percentage of the overall capital costs, then the amount of capsules required to operate at this departure delay should be constructed.

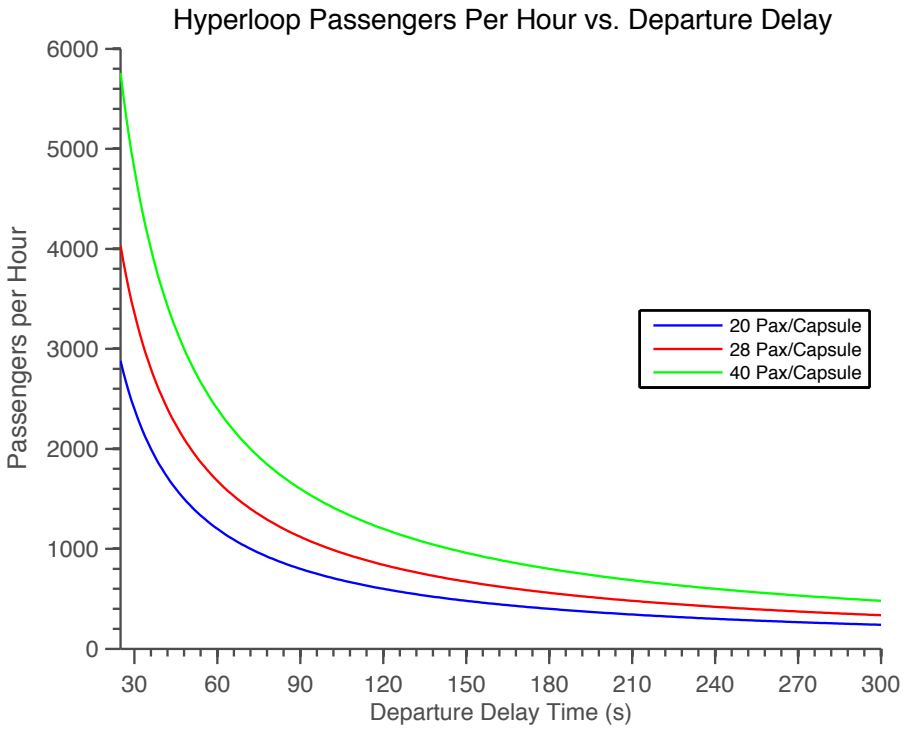



Figure 9.8: Number of passengers per hour as a function of departure delay with capsule capacities 20, 28 ($\alpha$), and 40 passengers.

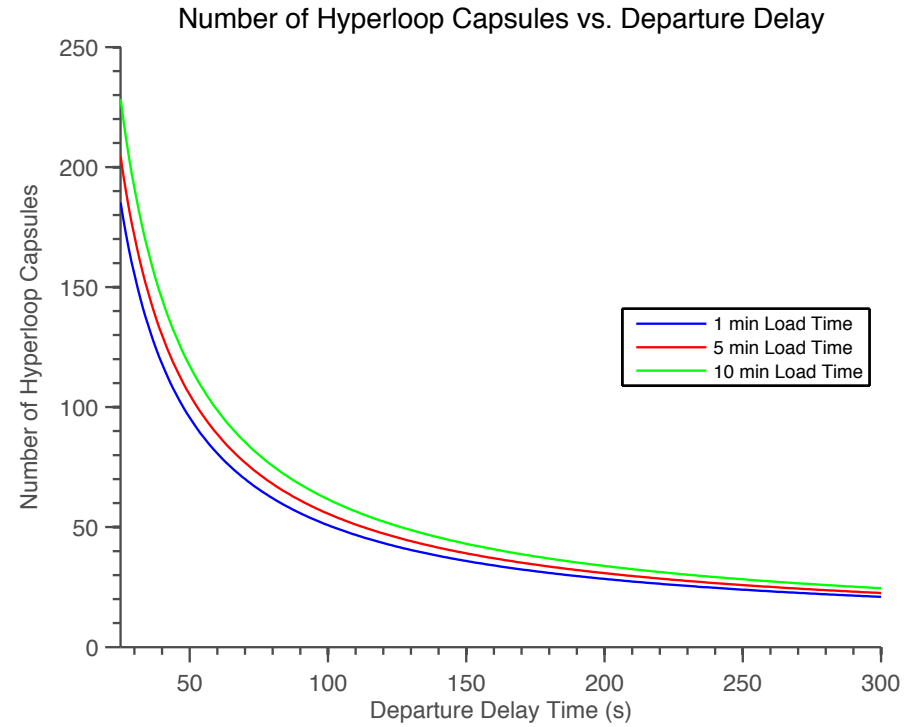



Figure 9.9: Number of capsules required for a given departure delay time with load times 1 min, 5 min, and 10 min.

## 9.3 Track Bend Radius: In-Depth Look

The track bend radius defined by the existing roadway limits the capsule's speed in certain sections of the track in order to maintain passenger comfort. Earlier, the bend radii of each section and the corresponding speed was taken from the alpha document recommendations. Now, the track path is looked at more closely to observe the lateral $g$-force on passengers throughout the trip. Using geographical data points of the route taken from Google Earth and computing the bend radius from parabolic curve fitting estimates, the lateral acceleration over the trip could be plotted.

The bend radius of a curve is defined as

$$\rho(t) = \frac{|1 + f'^{\,2}(t)|^{3/2}}{|f''(t)|} \tag{9.3.1}$$

where $f(t)$ is the route path. The equation for the route path can be estimated by a parabolic curve fitting method for a group of route points. The lateral acceleration can then be found from

$$a_{g,trans} = \frac{u_e^2(t)}{\rho(t)} \tag{9.3.2}$$

Using a technique developed by MathWorks to eliminate redundant route data points and lightly smooth the curve, the following lateral $g$-force plot can be developed (Figure 9.10) [4]. It can be seen there are several sections that exceed $0.5g$ where the Hyperloop alpha document listed this would not happen. The route path would need to be altered in these sections, requiring more land to be bought and potential destruction of existing structures. In addition, it is apparent the lateral $g$-forces can change rather rapidly in the suburban sections. Although most of the accelerations are in the comfortable range, humans still do no like the constant acceleration changes. This transportation system will not be very successful if it mimics a roller coaster.

A section of track that requires smoothing was examined in order to evaluate how much land may need to be acquired to make a more comfortable ride. While moving away from the interstate in the middle section of the journey will not be difficult, this could be very challenging in the suburban sections without encroaching on private property and displacing current infrastructure. High speeds may need to be sacrificed in the suburb regions. Total trip time will decrease, but passenger comfort will be maintained. An alternative is to have more active braking and propulsion during the suburbs, but this would add extra costs as well as potentially more passenger discomfort due to constant accelerations and decelerations. Maglev allows for easier

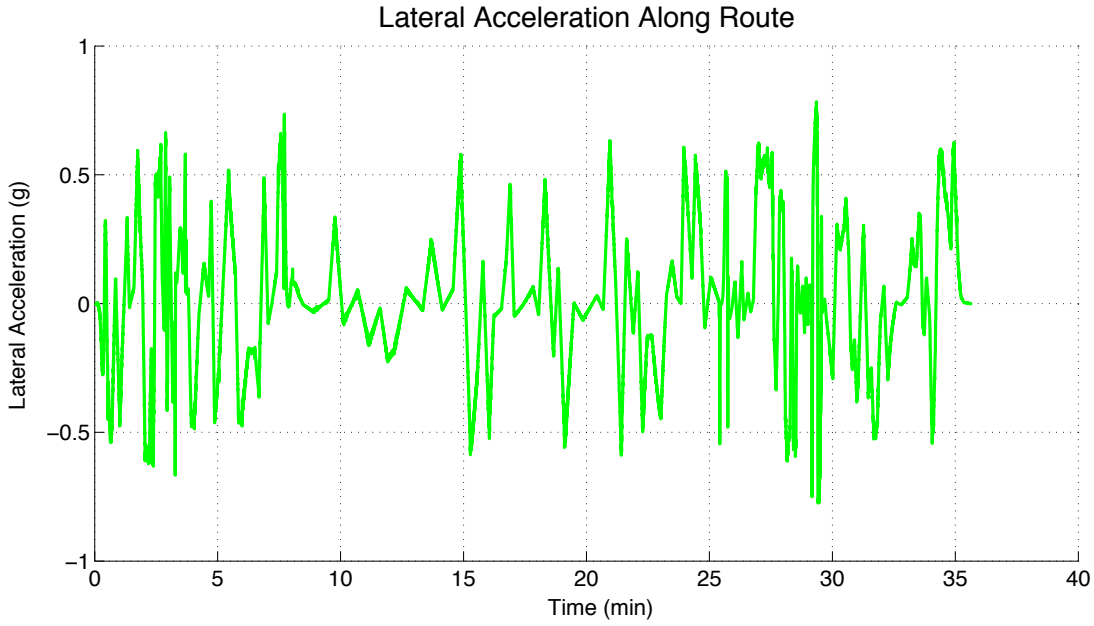



Figure 9.10: Lateral acceleration as a function of time from L.A. departure.

braking and re-accelerating, thus it is possible to use maglev only in suburban areas and then use air suspension system in the middle section to save on costs. However, there would be a significant increase in weight added to the capsule carrying both an air suspension system and maglev levitation system. A plausible alternative is to use a banking mechanism for the capsule as it goes around a turn. Yet, banking achieves less lateral acceleration at the expense of greater perceived vertical acceleration, which can give humans the sense of sea sickness. It may be possible to manipulate the height of the pylons to still reduce the resultant lateral accelerations while banking and transfer these to longitudinal, not vertical, accelerations that are tolerable.

Figure 9.11 displays the bend radius of an example track section if it were to exactly follow I-5. This snapshot is taken from a section where low speed ($u_{e,low}$) is suggested and the corresponding minimum bend radius is 3.67 km. All the turns in this displayed section are less than this minimum bend radius and thus, the track path will need to be altered. Figure 9.12 compares two options for altering the path:

1. Smooth track route so all turns have bend radii equal to 3.67 km (Figure 9.12a).

2. Make track route perfectly straight (Figure 9.12b).

The first option will correspond to the minimum land acquisition (5.49 km$^2$), while the second will correspond to the maximum land acquisition (14.18 km$^2$).

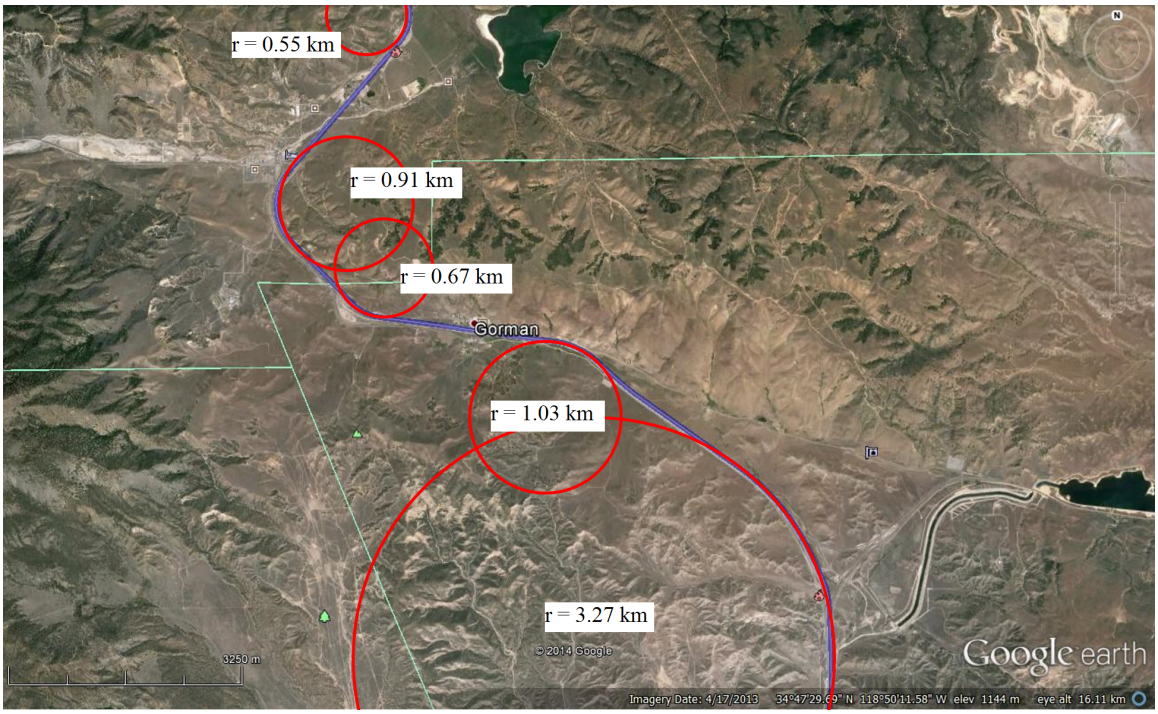
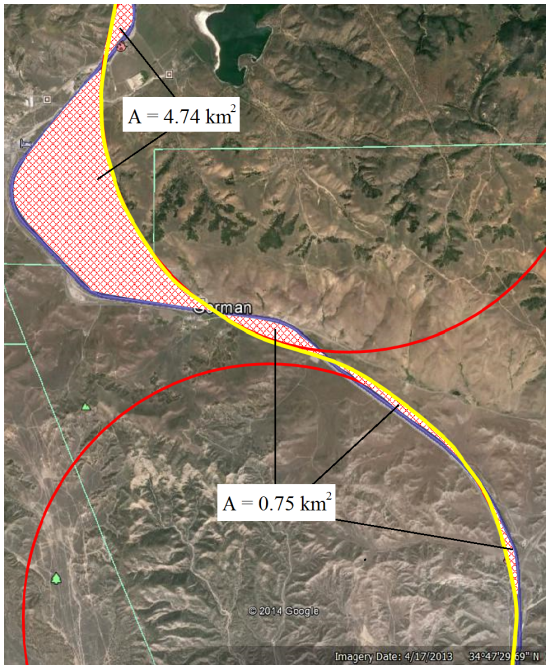
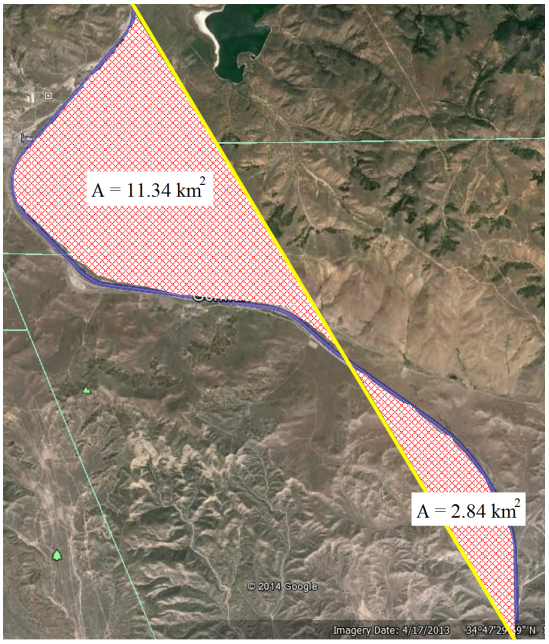



Figure 9.11: Example bend radii for route section with suggested low speed ($u_{e,low}$) and corresponding minimum bend radius ($r_{min}$) of 3.67 km.




(a) Area of land needed to acquire for track smoothing with turns made at $r_{min} = 3.67$ km.




(b) Area of land needed to acquire for making track perfectly straight.

Figure 9.12: Track smoothing and required land area. I-5 is displayed in blue, while the smoothed track is displayed in yellow.

An example of a suburban area where the Hyperloop route needs to be altered can be found in Figure 9.13. As the route approaches San Franscisco, the roadway I-580 takes a sharp turn. The bend radius of the roadway is only 0.59 km, which to only experience $0.5g$ would limit the speed to 53.84 m/s. To be able to travel at $u_{e,low}$ the track would need to be changed to have this speed's corresponding bend radius (red curve). Figure 9.14 takes a closer look into this section with the bend radius altered. It can be seen the Hyperloop route would need to go directly through The Neighborhood Church, an establishment which will not easily move regardless of the amount of money thrown at it. This is only one example out of many more established businesses or homes that will need to be displaced in order for the Hyperloop to travel at necessary speeds in suburban sections. An alternative option is to completely go around this suburban section. The yellow route in Figure 9.13 displays a potential alternative route. However, the diverted region contains many hills which complicates the pylon scheme for this section. These are tradeoffs that will need to evaluated in the preliminary design phase of the potential project.

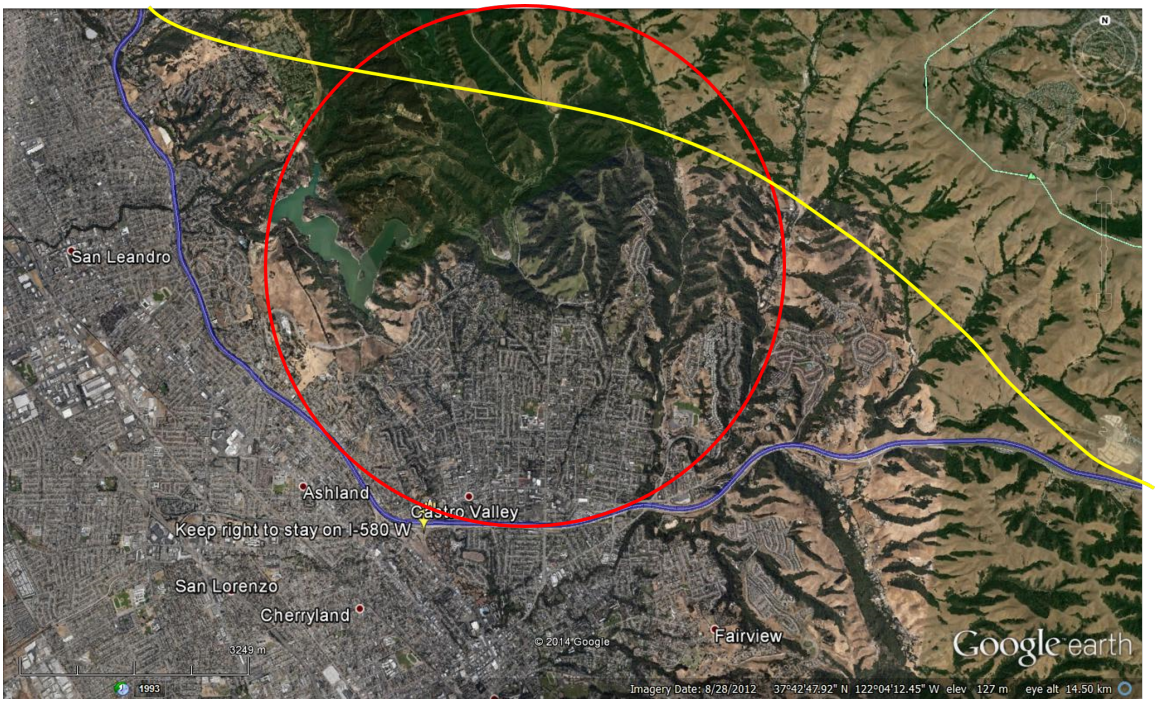



Figure 9.13: San Francisco surburban area where route path needs to be altered. The minumum amount of curvature needed for $u_{e,low}$ is a $r_{min}$ of 3.67 km (displayed in red). Alternatively, this suburban section can be diverted completely by moving the track north (yellow curve).




Figure 9.14: San Francisco surburan area that shows the minimum necessary altered path (yellow) to travel at $u_{e,low}$. This path goes straight through The Neigborhood Church.

## Estimating Costs

Estimating the capital costs associated with acquiring the land needed to make the Hyperloop route smoother and more comfortable for passengers while reducing overall travel time is very difficult. Land costs are expected to be cheaper in the middle section of the route where there is less established civilization. Obtaining the land here may be as simple as purchasing from an owner and then receiving a permit. The suburban areas are where it gets difficult to quantify the land acquisitions. The land will be much more expensive and the politics become much more complex. Many businesses and communities may not want to be displaced for the Hyperloop regardless of the amount of money offered to them. On one hand the California High Speed Rail project has estimated $3.915 billion in capital costs to purchase real estate and a total of $13.059 billion for sitework, right-of-way, land, and existing improvements [8]. On the other hand, the Hyperloop alpha document has only estimated $1 billion for permits and land. The reasoning for this low estimate is that since the Hyperloop will be elevated on pylons it can be placed in the median of the existing interstate system while only deviating from this roadway when necessary to reduce lateral $g$-forces. However, the alpha document completely ignores all the politics behind working with

the state government's Interstate Highway System division and constructing on or around their infrastructure. The highway would need to be shut down for long periods of time during the Hyperloop's construction and this would face much resistance from the government. While it is likely the Hyperloop can save money by building it alongside the interstate system, in order to maintain comfort and achieve low trip times the capital costs for obtaining land will be more comparable to the California HSR program's estimates. It will still be less because the high speed rail right-of-way is much wider than the Hyperloop tube. Other ways to reduce expenditures for land include using existing railway right-of-way. While this may not be as available in the L.A./S.F. corridor, there are other places in the country where this could be realized. There could even be a future where evacuated tube transport directly replaces old-fashioned trains for transporting large amounts of cargo and the existing railway right-of-way could be used. Another option to make mutually beneficial land transactions is to offer land owners a certain percentage of revenue generated across their section of land in exchange for perpetual right-of-way.

## 9.4 Summary

It was found that the aerodynamic analysis of the Hyperloop used by the alpha document team was too conservative. Using the aerodynamic model derived in Chapter 3, the revised total trip time was found to be 36.35 minutes (47 seconds longer than the alpha time). To be able make emergency stops at $1g$ without collisions, capsules can depart roughly every 30 seconds. For capsules with a capacity of 28 people, this corresponds to 3,722 passengers per hour each way and a requirement of $155 - 191$ capsules. Taking a closer look at the lateral accelerations throughout the route, it was determined significant alterations from the interstate system will need to be made in order to maintain passenger comfort (lateral accelerations below $0.5g$ and less frequent changes in acceleration). Large areas of land will need to be acquired to smooth the route path. This process will encounter more obstacles in suburban areas due to more existing infrastructure and resistance to displacement. The political and community effects surrounding land acquisition may be enough to delay the project and significantly increase the total costs. Solutions to managing the route in suburban areas include route detours, more frequent braking, lower speeds, and tunneling. The degree to which these route problems can be solved will be a driving factor of total costs and project scheduling.

# Chapter 10

# Hyperloop Infrastructure

## 10.1 Tube Route Layout Schemes

There are four possible tube route layout schemes for the Hyperloop. The tube can be built overhead on pylons, at ground level, shallowly below ground, or deeply below ground. Each method has its advantages and disadvantages. A study from Xijing University in China investigated the trade-offs between the different schemes [65]. The overhead scheme was the clear winner. While the underground methods are advantageous in respect to land acquisition and providing robustness to temperature and climate fluctuations, they are not realistic due to extremely high construction and maintenance costs. Tubes of the same size diameter would be much more expensive underground. Especially, since the costs of tunneling are much higher than those of building bridges. In addition, it is very difficult to check the vacuum state of the tube and then to fix a leak. The Swiss company SwissMetro proposed a completely underground vactrain that would be 50 meters below street level to connect Bern to Zurich in 12 minutes [44]. Even if these issues could be minimized and costs reduced, it would be hard to convince people to ride in a small tube embedded in the rock deeply underground where there is no easy escape in the case of an emergency. It is not surprising this concept has not gained much traction. Thus, the above ground solutions are more favorable.

The ground and overhead options will share many of the same advantages and disadvantages. The overhead option will face slightly higher construction costs due to pillar construction as well as some degree more of maintenance challenges. However, the estimated capital saved acquiring less land than the ground method gives the

overhead method the overall edge. Furthermore, tubes on the ground would be more exposed to damage by humans and natural occurrences like floods. Studies conducted for current Maglev projects also have corroborated that overhead transportation is optimal. Further civil engineering evaluation should be conducted for the specific region of interest. Factors such as the seismic activity in the California area could swing the scheme in one direction or the other.

## 10.2 Tube Material and Structure

There are two viable material/structure options that have been proposed with low cost and high reliability for evacuated tube transportation. The first is a pure steel tube. The second is a concrete composite structure with a thin metal layer. Differences concerning the manufacturing and construction of tubes with both materials will be discussed.

Technologies that depend on maintaining a vacuum environment typically use steel because it has good strength characteristics as well as low permeability to keep the tube sealed. The current price of steel is around $800 - $1000 per ton [11].

Concrete has low cost ($70 per ton), high compressive strength, and good stiffness, but it will not maintain the vacuum environment to the same degree as steel because it is porous [63]. However, gas-tight concrete has been used in nuclear reactor pressure vessels and seawater desalt jars for higher expenditures. The type of composite structure needed would feature a thin inner steel wall with an outer concrete layer. Because the inside steel layer will want to be pushed away from the concrete layer, special attention needs to be directed to securing it in place. This may be a challenge to avoid. The overall thickness of the tube may be larger with the composite structure, but the cost will be less since concrete is much cheaper than steel. This structure will have large compressive strength to allow for a more intense vacuum degree. A stainless steel layer could also be added to the outside of the concrete to help mitigate damage and corrosion. This layer would tend to be pulled against the concrete layer, making the fastening much easier.

## 10.3 Tube Thickness Numerical Analysis

In the field of mechanics of materials, a thin-walled tube is considered to be vessel having an inner-radius-to-wall-thickness ratio of 10 or more ($r/t \geq 10$). The stress

distribution throughout the thickness will not vary significantly so it can be assumed to be uniform [24]. Cylindrical vessels are subject to Hoop stress (circumferential stress) from the pressure differential established by the vacuum. The Hoop stress can be calculated from the following formula:

$$\sigma_{Hoop} = \frac{p_g \, r_{tube}}{t} \tag{10.3.1}$$

where $p_g$ is the gauge pressure, $r_{tube}$, is the inner radius of the tube, and $t$ is the tube thickness.

To design the tube thickness, the hoop stress multiplied by a factor of safety (FoS) is set equal to the compressive strength ($\sigma_B$).

$$t = \frac{\text{FoS} \cdot p_g \, r_{tube}}{\sigma_B} \tag{10.3.2}$$

For reasonable steel choices, $\sigma_B$ ranges from 180 MPa (stainless) to 1200 MPa (low carbon martensitic steel)[24] [11]. Using a FoS = 2, a tube with a diameter equal to 2.23 m (alpha diameter), the tube thickness needs to only equal 1.3 mm to 0.2 mm, depending on the steel chosen. This, however, is much smaller than what actually needs to be designed. Thin walls are subject to torsion deformation and destabilization. Zhang and Oster suggested tube thicknesses of 8-15 mm for a tube with diameter 2.4 m [63].

The tube should be designed to handle longitudinal stresses. This includes the bending stress induced by thermal expansion, bending stress induced by weight of tube (will be minimal since tube is simply supported), and longitudinal stress induced by internal pressure [17]. The bending stress is equal to

$$\sigma_{BL} = \frac{M}{I} = \frac{32DM}{\pi((D+t)^4 - D^4)} \tag{10.3.3}$$

The moment due to thermal expansion can be found from

$$M_{therm} = \frac{6EI\Delta L}{L^2} \tag{10.3.4}$$

where $E$ is the Young's Modulus, $I$ is the area moment of inertia, $L$ is the length of tube considered, and

$$\Delta L = \alpha_l L \Delta T \tag{10.3.5}$$

The average temperature change in a day for the Los Angeles area in 2013 was 8.3 K. Assuming the coefficient of thermal expansion for steel is $\alpha_l = 13$ x $10^{-6}$ m/m-K, the maximum $\Delta L$ can be computed. For a 30 m long section of tube (distance between two pillars), the maximum change in length is only 3.237 mm along its length. For a 20 mm thick tube the expansion radially is only 0.003 mm. Thermal expansion will not be a major concern for the safety of the tube wall as long as expansion joints are incorporated throughout the length of the tube.

The shear (torsional) stress the tube must withstand is

$$\sigma_T = \frac{TD}{2J} = \frac{32\,T\,D}{\pi((D+t)^4 - D^4)} \tag{10.3.6}$$

Expected torsional moments, $T$, can be plugged into this equation and used to check the thickness of the tube selected. Due to limitations in analysis time, a complete structural analysis with simulations was not completed. It will therefore be assumed the tube thickness is 23 mm for a tube of diameter 2.23 m (alpha conditions) and will scale with a change in tube diameter in accordance to the Hoop stress relationship. For example, a 6 m tube would correspond to a 65.53 mm steel tube thickness.

## 10.4 Pylons, Expansion Joints, and Dampers

The alpha document presented a basic structural model for the pylons needed to support the Hyperloop tube and mounted solar arrays. Reinforced concrete pylons will support and constrain the Hyperloop tube in the vertical direction, while allowing longitudinal slip for thermal expansion as well as dampened lateral slip to mitigate the effects of earthquakes. Less frequent expansion joints are needed than ground structures because the tube does not need to be rigidly fixed at any point. Two adjustable lateral (XY) dampers and one vertical (Z) damper can be placed inside the pylons, isolating the ground movements and thus, mitigating earthquake risk. The thermal expansion slips will be placed at stations where speeds are lower. The distance between pillars will be 30 m to reduce tube deflection effects and increase resistance to seismic loading. There will be roughly 25,000 pillars with a nominal height of 6 m. The alpha document team performed limited structural simulations on the model described and claimed the capability to withstand atmospheric pressure, tube weight, and earthquakes. These simulations were minimal and more in-depth modeling/simulating needs to be done. Specifically, more attention needs to be spent

on the effect of earthquakes. It is likely more analysis will reveal the need for more dampers and expansion joints in more frequent concentration along the tube length.

Earthquakes can be designed for, but this design will likely contribute to higher costs. The Trans-Alaska Pipeline runs across the Denali Fault and was designed to handle a maximum expected event reported from geological studies. When a 7.9 magnitude earthquake struck the pipeline in 2002, the design held and not a single drop of oil spilled. While a few supports were damaged, the piping remained intact. The engineering solution to accommodate the projected fault movement and intense earthquake shaking was to support the piping on Teflon shoes that are free to slide on long horizontal steel beams. This only added $3 million to the total cost when built in the 1970s, and saved potentially $100 million in repairs [60]. While air molecules may more easily escape a damaged evacuated tube than oil molecules, earthquakes risk can be designed for in the Hyperloop. Furthermore, earthquake risk applies to everything from transportation to buildings. With any type of infrastructure in earthquake zones, some risk has to be accepted and expected damage accounted for in its lifetime.

## 10.5 Large-Scale Engineering and Infrastructure Projects

Constructing the Hyperloop will be a massive engineering project. As with any large project there will be unaccountable factors and unknowns that appear throughout the project's development. The Hyperloop is likely to encounter similar setbacks to what caused California's $68 billion high-speed rail system to go far over budget. Political and community pressures will be major players. Lessons can be learned by examining past projects that have both succeeded an failed.

### 10.5.1 Princeton Plasma Physics Laboratory and Engineering Costs

The Princeton Plasma Physics Laboratory (PPPL) shared some engineering cost lesson learned from the challenges of their National Compact Stellarator Experiment (NSCX) [55]. Technical challenges manifested themselves throughout all phases of the project (design, R&D, fabrication, assembly) and led to the Department of En-

ergy (DOE) ceasing to fund the project. The factors contributing to the cost increases included complex geometry, tight tolerances, material requirements, and performance requirements. The magnitude of cost growth from the project baseline was investigated. It was found that there was 3.0 factor increase for design, a 1.3 increase for R&D and prototyping, a 2.3 increase for fabrication and assembly, and a 1.8 increase for procurement. The total factor of increase was 2.0. Geometry accounted for 35% of the increase, while accuracy accounted for 37%. Very tight assembly tolerances led to the need for sophisticated metrology equipment and metrology dedicated technicians, engineers, and analysts. The tolerance requirements were not well understood when the budget was established because certain components were not prototyped.

The lessons learned from this project will apply to the Hyperloop. A premature establishment of a firm cost and schedule baseline should be avoided until a more mature design and fabrication base can be developed. Tight tolerances may be necessary with Hyperloop tube due to the very small suspension gap height. These tolerances should be applied surgically and only where they are critical. Tolerances drive vendor procurement costs, require in-house engineering time to disposition nonconformance reports (NCR's), and increase assembly time. Labor costs are not cheap and large management may be required in addition. The analysis time to determine if the measured variation is meaningful is often underestimated. Prototyping is critical to account for all aspects of assembly. Simplifying the design can mitigate cost growth. Finally, it is important to recognize the nature of high tech/high risk projects and avoid prematurely establishing cost and schedule baselines until a more mature design/fabrication experience base is established. The government and most other investors are very risk adverse so when costs of a new technology start to exponentially increase people will begin to lose faith and may end up canceling the project.

While this list is not exhaustive, there are other factors related to the Hyperloop's infrastructure. The tight tolerances are subject to temperature change so analysis will need to determine if variation is problematic. Compliance needs to be built into the design to ensure a smooth assembly process. Corrosion, espcially around joints, can also cause harm. The Keystone Oil-Pipeline accounts for 0.1 mm/yr in corrosion (80-85% in the joints)[17]. While running oil is significantly different than a capsule moving through air, corrosion still needs to be investigated. Since California is an earthquake zone, everything moves and much more detailed studies need to be conducted than the simple structural analysis presented in the alpha document. Environmental studies need to be conducted to ensure the area's ecosystem is preserved. Community members may also be upset by the visual impact created by a Hyperloop

system. The next professional design evaluation of the Hyperloop needs to factor in all the risks and unknowns. This was not considered in the alpha proposal.

### 10.5.2 Other Large-Scale Infrastructure Project Costs

Large-scale infrastructure projects bring substantial impacts on communities, environment, and budget. While costs are astronomical, they can help boost local economics and create jobs for thousands of people. Environmental issues will contribute to the political sphere. Large infrastructure projects almost always cost more than the initial projections. A 2002 Danish study by Bent Flyvbjerg, Mette Holm and Soren Buhl looked at 250 major infrastructure projects dating back to the 1920s and found that roughly 90 percent of them went over budget by an average of about 45 percent [18].

Oil Pipelines are examples of large-scale infrastructure projects with similar structures to to the Hyperloop tube, but with less performance constraints. The Trans-Alaska Pipeline consists of a 1.22 m diameter piping system spanning 1,287 km with 11 pump stations. In 1969, the proposed cost was listed to be $900 million [32]. The final construction cost totaled $8 billion, while enlisting the work of 70,000 people. The entire Keystone Pipeline project (the existing 2,615 km plus the 1,897 km of KXL) is projected to cost $13.2 billion to build [12]. TransCanada has stated that $6.2 billion has already been used to establish the current infrastructure and $7 billion more is needed to complete KXL. The completion of this addition is currently a controversial issue. These oil pipelines mainly build on open land where existing structures will not interfere. The Hyperloop route will not have as much luxury, especially when approaching urban areas.

To examine the costs of massive infrastructure projects in heavily populated areas, the Big Dig (Central Artery/Tunnel Project) in Boston, Massachusetts was examined. The Big Dig rerouted the Central Artery (I-93) through the heart of the city by using a 5.6 km tunnel and establishing a wider roadway. In addition, the project included the construction of the world's widest cable-stayed bridge, the deepest underwater connection in North American, extensions of I-90, and many other infrastructure refinements. The project commenced in 1991 and it proved to be on of the most technically challenging urban transportation developments in the U.S. Originally estimated to cost $2.8 billion ($6.0 billion with inflation) and be finished by 1998, upon completion in 2007 the project was estimated to have cost $14.8 billion [35] [46]. The actual cost was released to the public in 2012 with a total more than $24 billion,

earning the title as the most expensive highway project in the U.S. The scale of this project compares to the Panama Canal and the Channel Tunnel. While this example may be on the extreme side, it does show how dealing with a massive project in heavily populated areas can lead to significant cost and time increases. There will always be unknown variables that are not accounted for at the project's start, and dealing with the problems that arise will be more challenging in urban sections. The Hyperloop will not have much trouble in between Los Angeles and San Francisco, but as the route enters either city there is a whole array of different factors to consider and the challenges they bring will be hard to predict.

## 10.6 Hyperloop Infrastructure Costs

### 10.6.1 Tube Costs

It is assumed the tube will be constructed of steel costing $800 per ton. The alpha document tube has a diameter of 2.23 m and a thickness of 23 mm. To examine the effect of increasing diameter, the tube thickness will scale with diameter defined by the Hoop Stress relationship. Estimates of welding and installation cost is taken to $800,000 per km [63]. The following raw material costs plus welding and installation costs for the Hyperloop tube can be found in Figure 10.1 as a function of tube diameter. These estimates for raw material costs plus welding and installation costs are larger than the extrapolated alpha costs for tube construction. For the alpha document's passenger system diameter, the revised cost is $1.1 billion compared to $650 million for the alpha. These new cost estimates may still be conservative. Tooling can rapidly increase with scale factor, so the tube costs may increase with $D^3$ instead of only $D^2$. In addition, the cleaning and boring machine discussed by the alpha document to smooth the inside of the tube will need to be custom made, and depending on the tolerances desired this may add a substantial expense.

### 10.6.2 Pylon Construction Costs

The alpha document predicts pylon construction will cost $2.55 billion. This likely is an underestimate because it is assuming these pylons are identical pieces that can be mass produced and dropped in place. Since the landscape varies rather significantly in this region the pylons will need to vary more in order to keep the vertical accelerations experienced by the passengers constant, requiring more custom manufacturing.

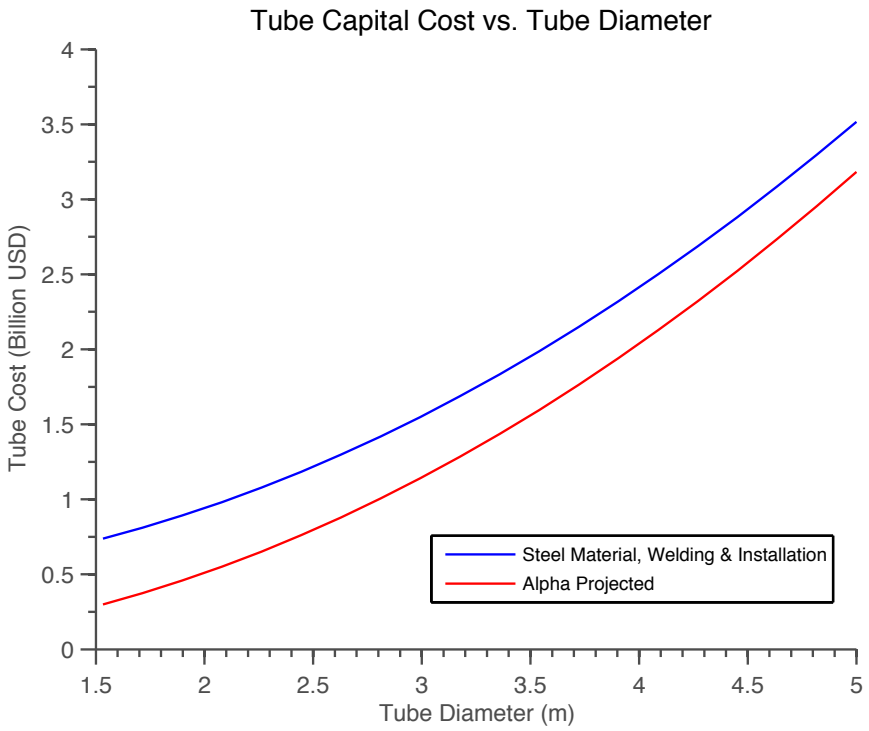



Figure 10.1: Tube costs as a function of tube diameter. The sum of the pure steel material costs plus welding and installation costs is plotted in blue. This is larger than the alpha projected tube construction costs (red).

The California High Speed Rail anticipates nearly ten times the cost for viaducts (pylon structure) than the alpha document [8]. The CHSR lists an average of $44.39 million/km (including contingency) for viaducts versus $4.53 million/km for the Hyperloop. It should also be considered that after a budget review from 2009 to 2012 the CHSR increased the budget for viaducts by more than a factor of 2 [9]. However, it is hard to compare the Hyerloop pylons to the CHSR because their structures have fundamental differences. The high speed rail's viaduct will need to support significantly more mass. The Hyperloop will feature similar superstructure (below ground) to the CHSR, but the substructure (above ground) will be different. It is a good assumption to consider the Hyperloop pylons will cost somewhere between the alpha proposal and the CHSR 2012 viaduct budget, with the revised cost being closer to the alpha document end. It is then assumed the pylon cost will be 3 times the alpha projection due to more customization than originally anticipated and the evidence that original projected costs will at least increase by a factor of 2 from initial budget. Therefore, a suggested estimate for pylon costs is $13.59 million per km for a total of $7.65 billion for the entire Hyperloop pylon construction. This is already larger than

the total alpha cost of $6 billion. It is also assumed that pylon cost is only a weak function of tube mass.

### 10.6.3 Tunneling Costs

Tunneling for the Hyperloop route can be expensive. The alpha document estimated 24.2 km of tunneling for where extreme local gradients are greater than 6%. The estimations state tunnel construction will cost $600 million ($24.8 million per km). The California High Speed Rail estimates tunneling to cost a total of $13 billion ($168.32 million per km), more than double the total from the 2009 business plan (though the cost increase per km was only about 6%)[9]. The Hyperloop may find it will need to tunnel underground in the urban areas to avoid displacing infrastructure. This will increase costs similar to what was seen from the CHSR 2009 budget to the 2012 budget. Still, the Hyperloop tunneling costs will be much less than those of the CHRS due to the much smaller bore size needed. As a result, less concrete reinforcements will be needed. The CHSR investigated the methods of tunneling. They found there is not a significant cost difference between using tunneling bore machines and drill/blast methods. However, the drill/methods take longer so a tunneling bore machine would be preferred. Ted Zoli, National Bridge Chief Engineer at HNTB Corporation, discussed how the tunneling for the Hyperloop could be done with a custom horizontal directional drilling (HDD) unit [1]. While the largest used can only bore out 64% of the required Hyperloop diameter, a custom unit could be built. Still, the question remains if the time and costs to make a larger device will be less than the alternate drill/blast method. Doubling the length of tunneling needed for the Hyperloop and adding the cost of developing a larger boring machines, it is suggested the total tunneling costs will be around $1.5 billion ($31 million per km). This cost will scale with the area needed to bore for the given tube diameter.

There are several other unknowns that can contribute to the civil infrastructure costs. For example, the alpha document suggests the Hyperloop will not cross the San Francisco Bay. If this will be added to the route, there will need to be either a bridge or a tunnel underneath the waterway. For now, this expenditure will be ignored to keep cost evaluation consistent with the alpha document.

## 10.7 Total Civil Infrastructure Costs Summary

The total civil infrastructure costs were broken down and analyzed using other large-scale infrastructure projects. These costs consist of the tube construction costs, the pylon construction costs, and the tunneling costs and are plotted in Figure 10.2. For the alpha tube diameter of 2.23 m, the total civil infrastructure costs alone reach a total of $10.2 billion, 2.7 times the same cost predicted by the alpha document. Even without considering the other capital costs, this is larger than the alpha document's predicted $6 billion total capital expenditure for the entire Hyperloop system. The other capital costs that need to be consider include everything associated with the capsule, propulsion, solar panels and batteries, vacuum pumps, and land acquisition. This will be discussed in the next chapter.

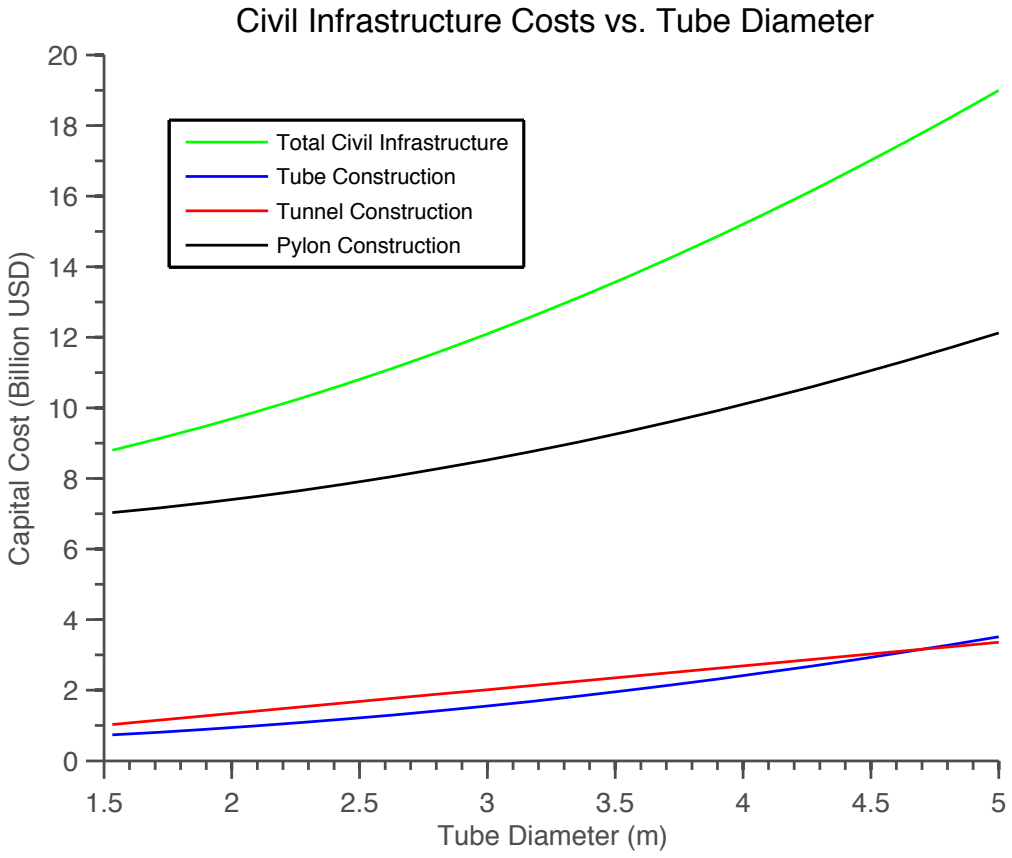



Figure 10.2: Total civil infrastructure capital costs as a function of tube diameter.

# Chapter 11

# Effect of Changing System Parameters on Overall Trip Time and System Costs

## 11.1 Introduction

Using the analyses from the previous chapters, the effects of changing several system parameters on overall trip time, system operational costs, and system capital costs were examined. Alpha document conditions were held constant while the selected parameter was allowed to vary. The assumptions for the route used to calculate the total trip time are the same as in Chapter 9.

## 11.2 Effect of Changing Tube Diameter

The tube diameter proposed by the alpha document is very small (only 2.23 m). Many humans may find it uncomfortable to ride in a capsule that is only 1.35 m tall. The alpha document also discussed the possibility of building a larger system that could transport cars as well as passengers. First, the effect of increasing the tube's diameter on the overall trip time is investigated holding the capsule size and everything else constant. Second, the possibility of creating a larger Hyperloop system which may be more comfortable for riders and even be able to transport cars is explored. In the latter case the capsule will scale with the tube diameter (constant blockage ratio).

Overall trip time will not be impacted as much as capital and operational costs.

## Overall Trip Time - Variable Blockage Ratio

If the tube diameter is increased, holding everything else constant it is expected that the overall trip time should decrease because the blockage ratio decreases and thus, the aerodynamic drag is less. The effect can be observed in Figure 11.1. It is interesting to note the time stays between 35 min and 39 minutes for blockage ratios 0 to 0.7. Thus, at the low pressure of 100 Pa, the blockage ratio does not have a significant impact on the overall trip time. However, once the flow becomes choked for blockage ratios larger than 0.7, the total trip time will more dramatically increase.

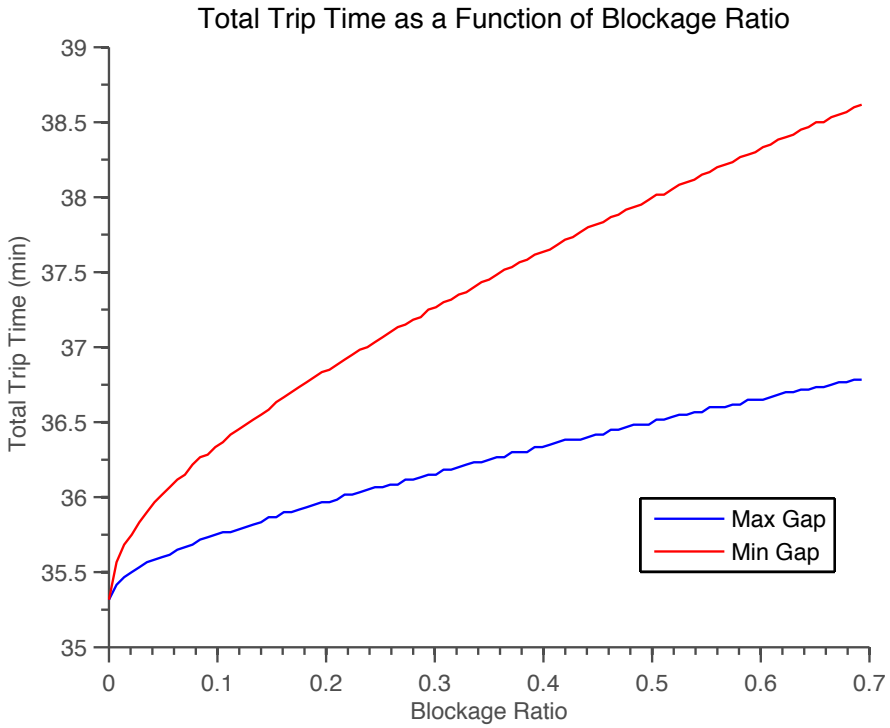



Figure 11.1: Total trip time as a function of blockage ratio.

## Overall Trip Time - Increasing Tube and Capsule Size

If a larger Hyperloop system is desired, the effect of increasing both the tube diameter and capsule size while holding the blockage ratio constant can be observed to evaluate this proposition. It is assumed the tube diameter directly scales with both the frontal surface area and the capsule mass. Only the the width and height

of the capsule change (maintaining constant aspect ratio), while the capsule length remains constant. From Figure 11.2 the total trip time actually decreases slightly as the overall system size is increased. This suggests that the the increase in mass of the capsule outweighs the increase in total aerodynamic drag force, and thus there are slower changes in accelerations.

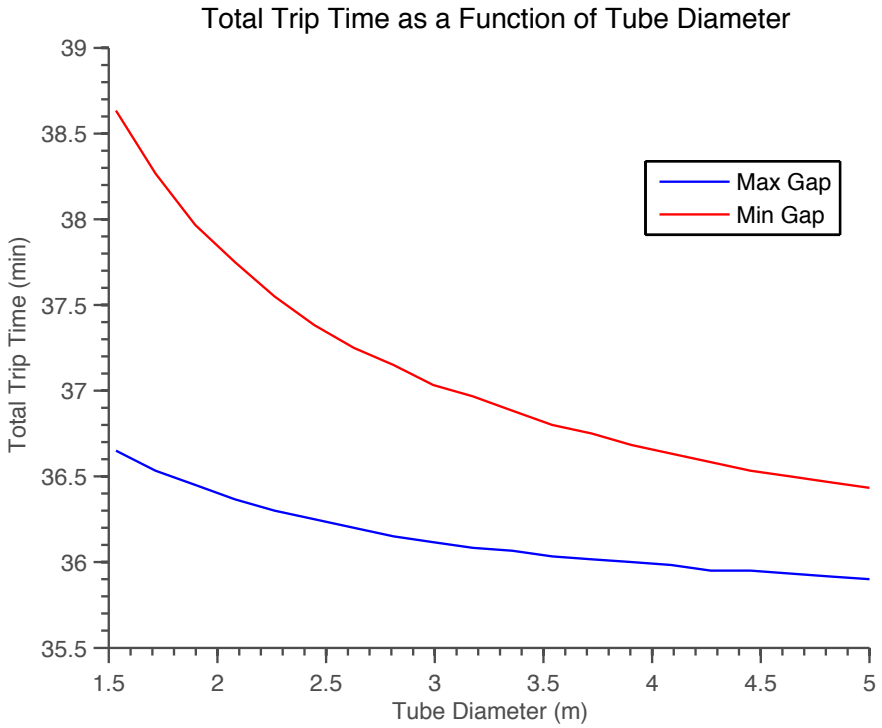



Figure 11.2: Total trip time as a function of tube diameter.

## Operational Costs - Increasing Tube and Capsule Size

When the overall system size is increased the total trip slightly decreases, but the energy required for the propulsion sections will increase dramatically (Figure 11.3) due to the larger mass of the capsule and larger aerodynamic drag from the increased capsule surface area. This increase will scale directly with operating costs of the system. There will come a point where the solar arrays cannot supply the necessary power and instead, power will need to be drawn from the grid. This will be much more expensive and also pose a risk if the grid goes offline. Larger systems will feature higher fares as a result.

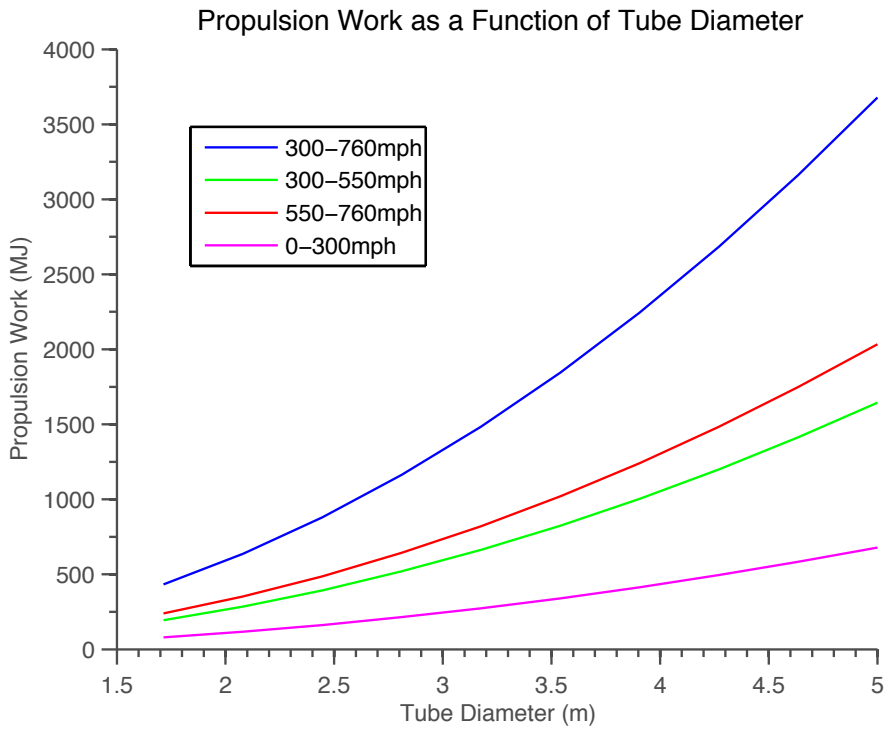



Figure 11.3: Propulsion energy as a function of tube diameter. The capsule size and mass scale with diameter. The four propulsion segments are plotted.

## Capital Costs - Increasing Tube and Capsule Size

The previous chapter should be consulted for the breakdown of civil infrastructure capital costs as functions of tube diameter.

The capital costs associated with the capsule will be based on the alpha document presentation (Table 2.1). The estimated total costs for 40 passenger-capsules and a tube diameter of 2.23 m is $54 million. Manipulating the costs presented for the cargo capsule and passenger capsule of the 3.30 m tube diameter passenger-plus-cargo system, 40 passenger-capsules are estimated to cost $62 million. Assuming these costs scale as the tube diameter squared, costs for other configurations may be estimated.

From Chapter 9, it was discussed that the configuration that best balances maximizing passengers transported and minimizing number of capsules required is for a departure delay of 50 seconds, corresponding to 2,016 passengers transported per hour and 105 capsules required (5 minute load time and 28 passengers per capsule). Thus, for 105 capsules and tube diameter of 2.23 m the capital cost of capsules will be $141.75 million. This is not a large percentage of the overall capital costs and therefore, it is recommended to build the number of capsules needed to maximize

passengers transported for $1g$ maximum emergency deceleration. For a departure delay of 30 seconds, load time of 1 minute, and 28 passengers per capsule, 3,360 passengers can be transported per hour using 155 capsules, raising capsule capital costs to $209.25 million.

## 11.3 Effect of Changing Capsule Length

Longer capsules may be desired to transport more passengers, impacting both trip time and costs.

### Overall Trip Time - Increasing Capsule Length

Increasing the capsule length (and mass) while holding all the other alpha parameters constant leads to a minimal decrease in overall trip time (Figure 11.4). Like scaling the entire system up, when the capsule length is increased, the increase in capsule mass outweighs the increase in aerodynamic drag from the larger bottom surface area. The capsule decelerates slower for longer capsule lengths.

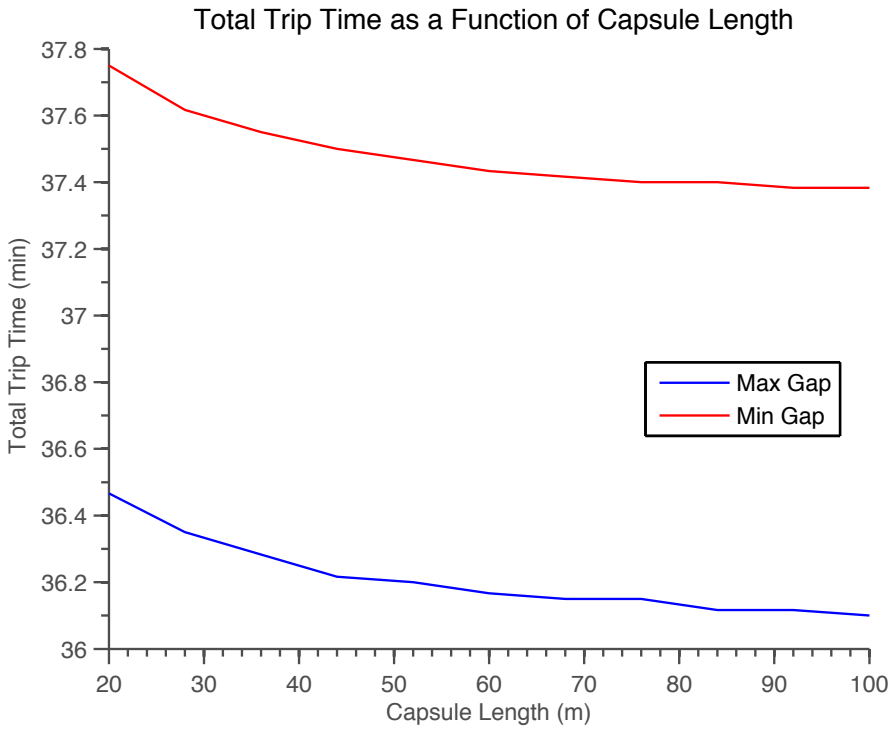



Figure 11.4: Total trip time as a function of capsule length.

## Operational Costs - Increasing Capsule Length

The larger mass and aerodynamic drag associated with an increase in capsule length leads to significant increases in required energy input (Figure 11.3). Another issue

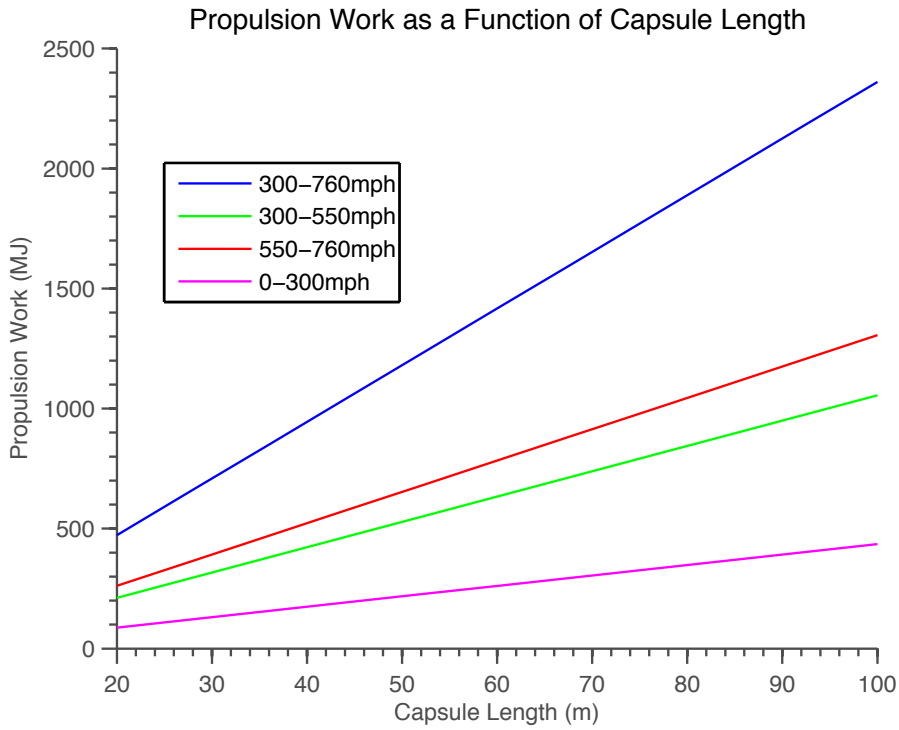



Figure 11.5: Propulsion work as a function of capsule length for max suspension gap height. The four propulsion segments are plotted.

with larger capsules is the increased mass will require a larger lift force for suspension. This will require more compressed air input from the air bearing suspension system. There will be a limit to the amount of air supplied as well as increased power requirements for the compressor machinery.

## Capital Costs - Increasing Capsule Length

The capital cost of capsule are assumed to increase linearly with increased capsule length (Figure 11.6). This scheme only considers 40 capsules. A similar trend would be seen for increasing the frontal surface area of the capsule.

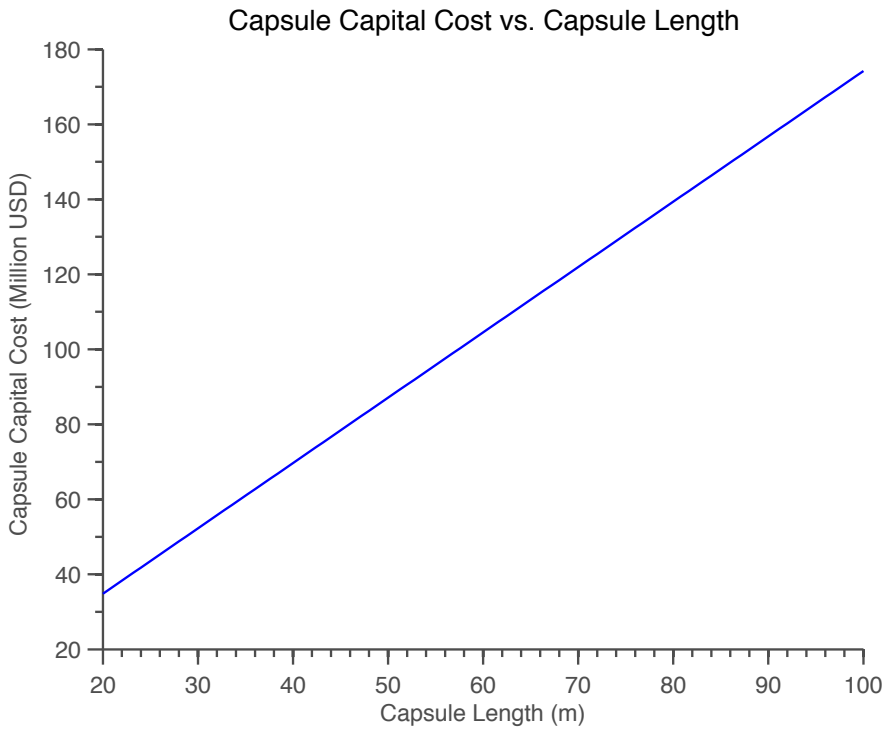



Figure 11.6: Capsule capital costs as function of capsule length.

## 11.4 Effect of Changing Tube Pressure

The tube pressure is one of the most important parameters in the Hyperloop system. Evacuating the tube to a low enough vacuum degree will significantly decrease aerodynamic drag and allow the capsule to coast and maintain speed for most of the journey.

### Overall Trip Time - Tube Pressure

Varying the tube pressure from 0 Pa to 10,000 Pa reveals the largest impact on total trip time (Figure 11.7). The total time varies from about 35 minutes to nearly 120 minutes for the max suspension gap curve. This range can be discussed in terms of hours, whereas the other parameters have been limited to a few minutes of deviation max. It is evident a tube pressure less than 2000 Pa will be necessary to make the trip in under 40 minutes. Figure 11.8 takes a closer look at the 0 to 500 Pa range. This plot shows that any of the pressures in the range will lead to a total trip time within 1 minute of each other for a given suspension gap curve. Thus, while 100 Pa may give the fastest time for the most manageable vacuum pumping scheme, a slightly higher pressure would produce similar results.

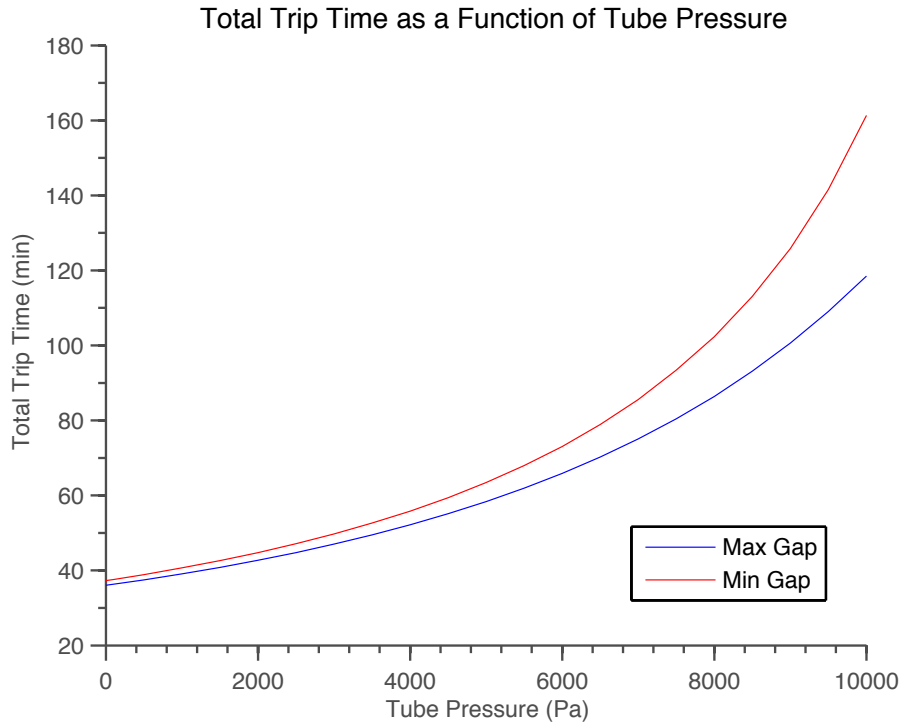



Figure 11.7: Total trip time as a function of tube pressure.

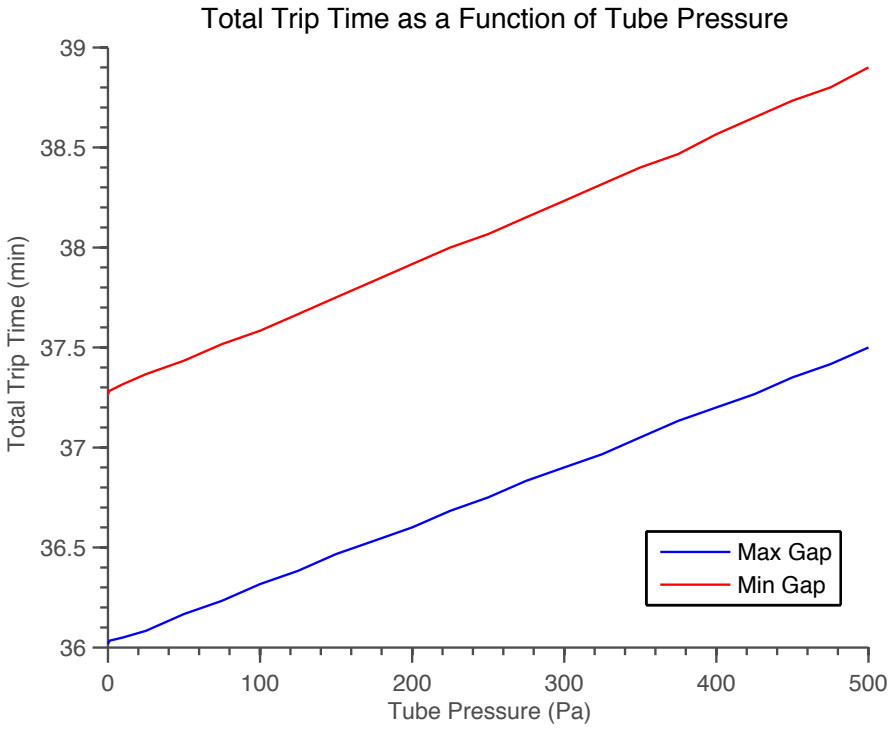



Figure 11.8: Total trip time as a function of tube pressure focusing on pressures 0 to 500 Pa.

## Operational Costs - Increasing Tube Pressure

For tube pressures below 10,000 Pa, an increase in pressure does not lead to a significant increase in energy requirements for propulsion of each station (Figure 11.9). However, significantly more propulsion stations will be needed at higher pressures to maintain capsule speed. Otherwise, the trip may take hours as seen in Figure 11.7.

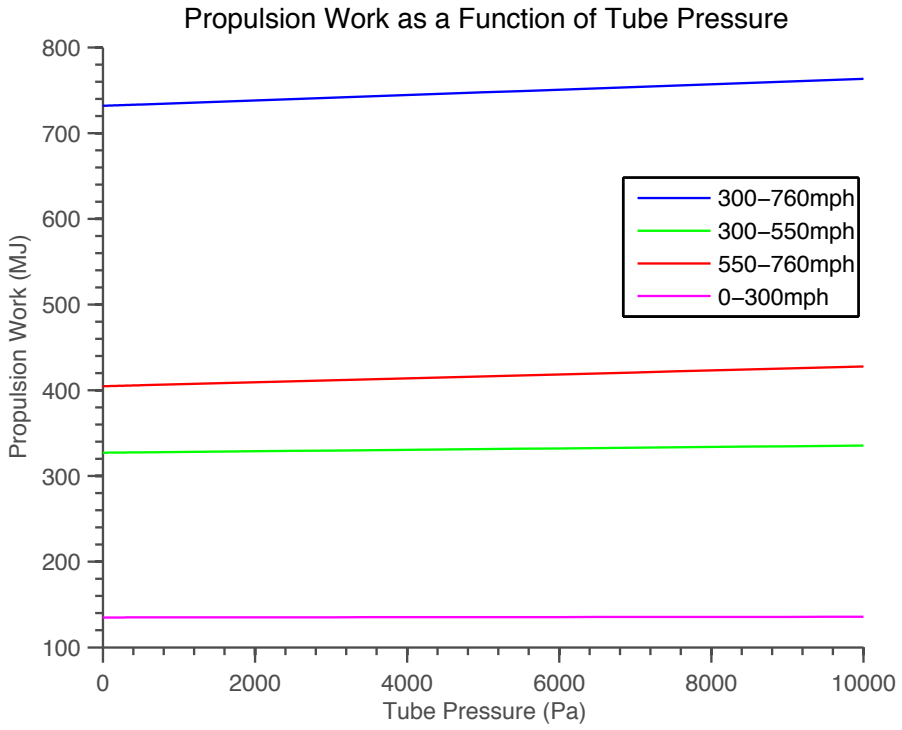



Figure 11.9: Propulsion energy as a function of tube pressure.

## Capital Costs - Increasing Tube Pressure

Vacuum capital costs will increase with decreasing target tube pressure. Higher vacuumizing speeds are required to keep pump-down times low, which need more complex vacuum machinery. Even assuming the $250,000 custom made Pfieffer vacuum (vacuumizing speed of 7500 L/s) will be used every 2 km for both directions of the tube, the total capital costs are only $140.75 million USD. Assuming more complex vacuum setups are required for airlock stations, more redundancy is wanted throughout the tube's length, and weather resistant stations are built for each pump, the total capital costs for vacuum pumps and stations will be very close to the $260 million USD published in the alpha document.

## 11.5 Effect of Changing Suspension Gap Height

The effect of varying the suspension gap height from 0 - 5 mm was analyzed under the assumption there is always enough compressed air to keep the capsule levitated in this gap range.

### Overall Trip Time - Suspension Gap Height

Figure 11.10 reveals a hyperbolic-like curve for total trip time with the knee occurring around 0.5 mm. If the gap is decreased beyond this point, the total trip shoots up rapidly. This point in the curve perfectly corresponds to the minimum gap height discussed in the alpha document. This result was obtained independent of the document. Similar to the alpha document a maximum suspension gap height around 1.3 mm would be suggested. The gains of a larger gap height are minimal in comparison to the substantial increase in compressed air input needed to keep the capsule levitated at those points.

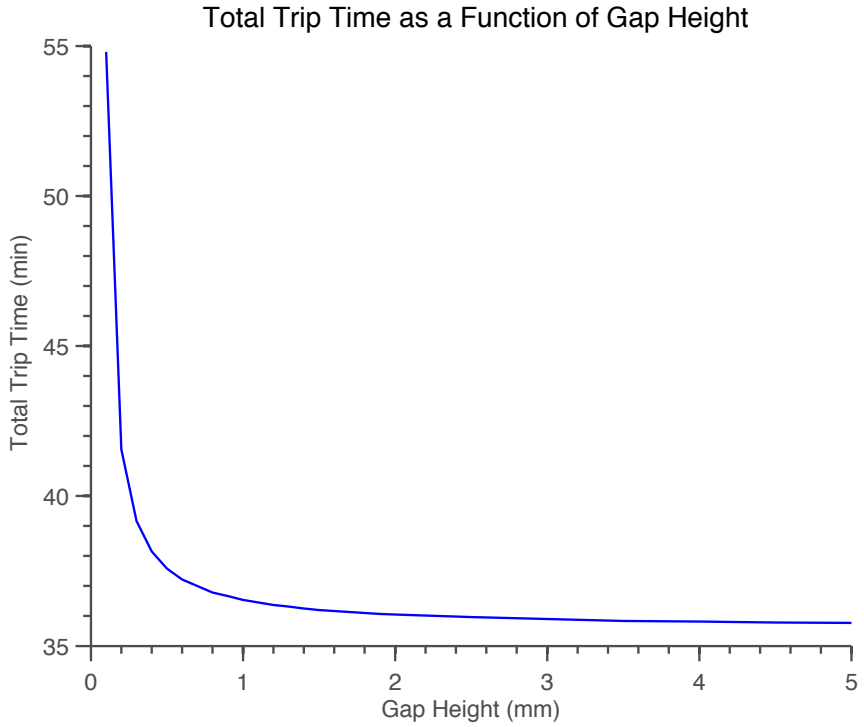



Figure 11.10: Total trip time as a function of gap height. Knee bend in the curve occurs around 0.5 mm.

## 11.6 Other effects

Changing the gap temperature (gap viscosity) led to a very small increase in trip time. The importance of this parameter has more effect on the materials of the suspension blades.

## 11.7 Total Costs

The total capital costs presented by the alpha document have been revised throughout this thesis. These findings are summarized in Table 11.1 for passenger Hyperloop system ($D_{tube}$ = 2.23 m). While the alpha document only incorporated a 10% cost margin, examining other large-scale infrastructure projects suggested it is more standard to add a 20% cost margin. This effect was implemented in the revised costs. It is also assumed that Solar Panels and Batteries will cost the same as the alpha proposal. The capital cost to acquire land is estimated to be three times the alpha cost. The stacked bar graph in Figure 11.11 visually depicts the increases in capital costs for each category. The revised total cost is suggested to be $16.84 billion USD versus the original alpha total cost of $6 billion USD. Even though the revisions nearly triple the alpha proposal they are still well beneath the $68.4 billion USD price tag for the California High Speed Rail. The revised costs may still be conservative in some areas while overcompensating in other areas.

Table 11.1: Total Capital Cost Comparison

| Component | Alpha Cost (Billion USD) | Revised Cost (Billion USD) |
|---|---|---|
| Solar Panels & Batteries | 0.21 | 0.21 |
| Station & Vacuum Pumps | 0.26 | 0.26 |
| Propulsion | 0.14 | 0.10 |
| Capsule | 0.05 | 0.21 |
| Tube Construction | 0.65 | 1.10 |
| Pylon Construction | 2.55 | 7.65 |
| Tunnel Construction | 0.60 | 1.50 |
| Permits and Land | 1.00 | 3.00 |
| Margin | 0.54 | 2.81 |
| Total | 6.00 | 16.84 |

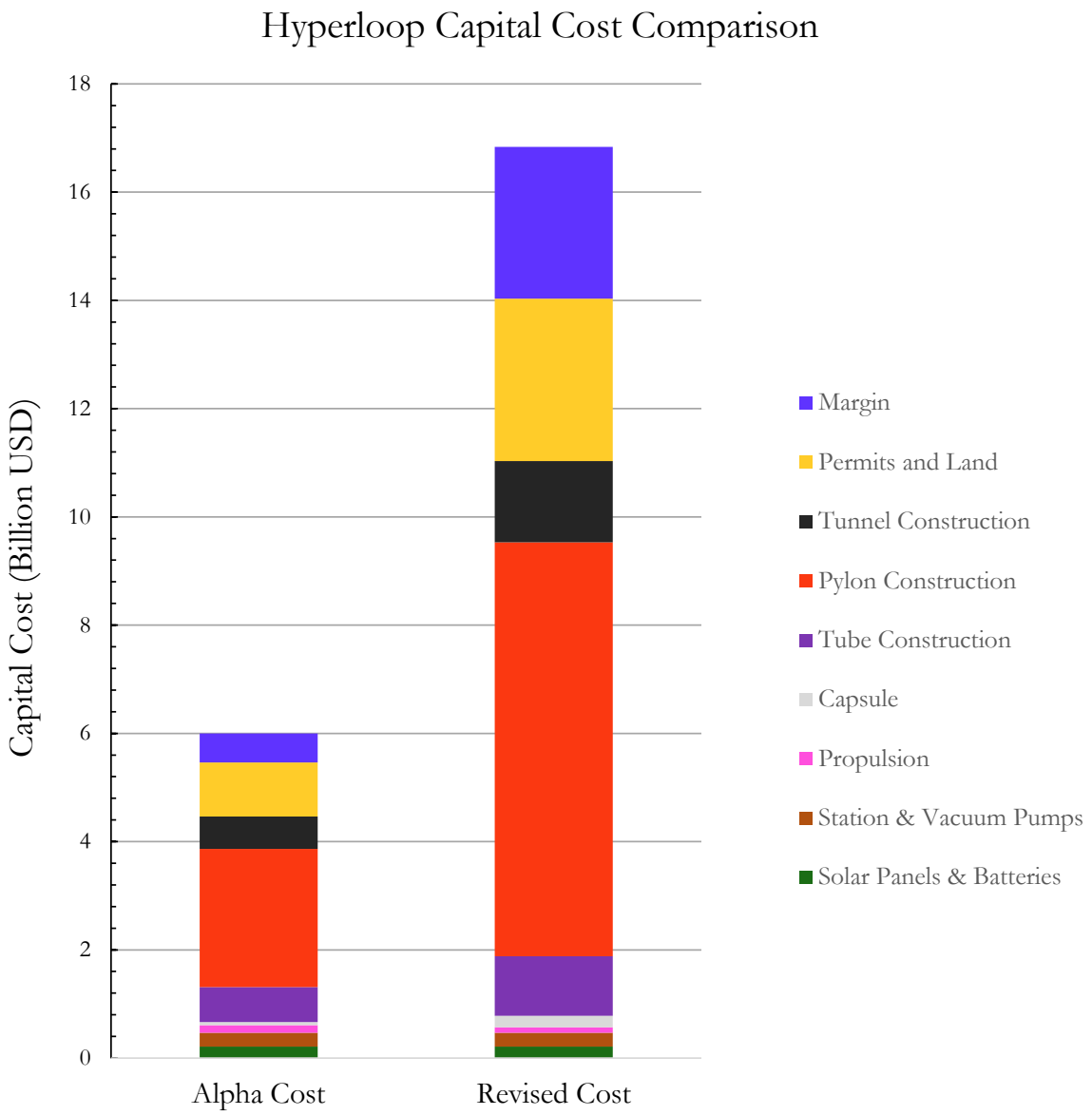



Figure 11.11: Capital cost comparison. Alpha total cost is $6 Billion USD vs. Revised total cost of $16.84 Billion USD.

In the end, funds should be invested into this mode of transportation if the net expected social benefit is both high enough to compensate for the infrastructure capital and operating costs and greater than the next best alternative. This will be strongly dependent on volume of traffic in the corridor, expected time savings, average willingness to pay of potential users, the release of capacity in congested roads, airports or rail lines, and the net reduction of external effects. Further studies are needed to more accurately evaluate this issue.

# Chapter 12

# Conclusion

Elon Musk provided an innovative spark to transportation technologies when he released an alpha document for a new mode of transportation called the Hyperloop. While the document provided a complete overview with clear goals for the system, more thorough engineering analysis was required to assess its technical viability as well as its economical reality. Each subsystem was broken down into its fundamental parameters and governing physical principles. These were then analyzed to evaluate their effect on both their corresponding subsystem and the overall Hyperloop performance. Several modifications were suggested to make the system feasible. Issues downplayed by the alpha document were brought to attention and their impacts were discussed. Economics, politics, and other human factors were also considered to complement the engineering analysis to gain a top-level perspective on this new mode of transportation.

The most important physical parameter needed to achieve the high speeds desired by the Hyperloop is the tube's pressure. The magnitude of the aerodynamic drag needs to be reduced to minimize energy input and to allow the capsule to coast for the majority of the journey. The previous chapter's analysis on tube pressure and overall trip time from Los Angeles to San Francisco showed that tube pressures around 10,000 Pa would take nearly two hours, while lowering the tube pressure to the alpha document's recommendation of 100 Pa would only take 36.35 minutes. The aerodynamics and vacuum technology analyses suggested lowering the pressure below 40 Pa would produce diminishing returns. An upper bound on the tube pressure can be established by a maximum permissible trip time. In order to make the trip in less than 40 minutes the tube only needs to be evacuated to 2000 Pa. Target tube pressure and desired pump-down times will dictate vacuum pump technology.

Keeping station interval distances small will help reduce pump-down times as well as introduce redundancy for better leak detection and fixes. Higher vacuumizing speeds are needed for airlock chambers.

Propulsion analysis acknowledged the effectiveness of the Double-Sided Linear Induction Motor (DSLIM) to accelerate the Hyperloop capsule to full speed and established the requirements for $1g$ acceleration. The Hyperloop aims to be self-powering by utilizing regenerative braking and solar energy. Mounting solar panels on top of the Hyperloop's tube was determined to be more than sufficient to handle the propulsion system's energy requirements, and the additional energy could be used by other subsystems such as the vacuum pumps or even sold for a profit. Reducing the operational costs due to energy will help keep ticket prices low. The capital costs of propulsion are dependent on the energy and peak power requirements. Because these costs are only a small percentage of the total capital costs, adding several reboost stations throughout the Hyperloop journey should be implemented to mitigate elevation changes as well as allow for more active speed control in the suburban areas.

The air bearing suspension system is the largest technical challenge of the Hyperloop. Even at high speeds, the aerodynamic lift created by the air bearing skis is not large enough to maintain vehicle levitation, creating the need for substantial compressed air input. This can be achieved through a higher pressure of the compressed air or a larger mass flow rate. High mass flow rates risk choking the flow in the small gap region and creating shock waves, while the higher magnitude of compressed air will require larger power and coolant requirements from the compressor system. Furthermore, the small gap will create the need for tight tolerances for tube manufacturing and assembly. A precise control system is essential to avoid collisions with the tube wall and to mitigate the risk of adverse effects similar to pilot-induced oscillations. Maglev is a proven technology seen operational in high speed train systems throughout the world and more consideration should given to using it for the Hyperloop's suspension. The risks of developing the air suspension system to a high enough standard for public transportation may be greater than the extra costs of using maglev. Due to ambiguous cost categories found in the existing maglev systems, the additional cost of implementing maglev in the Hyperloop was not accurately evaluated to be able to make a recommendation. It is imperative a more complete cost analysis is done on maglev technology before spending more time developing air suspension technology.

A compressor mounted on the capsule's front is needed to prevent the flow from becoming choked at the Hyperloop's high speeds. It was found a diffuser is needed

to ensure the flow does not become supersonic at the compressor's inlet. The heat released from the compressor system requires as larger water coolant mass flow rate than anticipated by the alpha document. The increase in the required water mass has effects that propagate through the entire system.

The ratio of the capsule size to tube size should be kept small in order reduce viscous drag and prevent the flow from choking. The overall tube and capsule size will drive total capital costs. It is suggested a larger system be built for more passenger comfort. User studies should be conducted where participants are required to sit in a mock capsule for the entire trip length. Ergonomic feedback will drive capsule size.

Although the technical aspects of the Hyperloop are challenging, it will be feasible to build an operational system. This will require a substantial amount of prototyping and design refinement. The recommendations made concerning the system's aerodynamics, propulsion, suspension, control, vacuum technology, compressor, route, and civil infrastructure can be used as a more developed foundation to advance Hyperloop work. While technical solutions will be found to ensure high performance and passenger satisfaction, it will be other aspects that have the potential to keep the Hyperloop from leaving the concept stage. Economics and community pressures will dictate the future of the Hyperloop in the Los Angeles/San Francisco corridor.

It was proposed for the route to run along I-5 to minimize land acquisition costs. The lateral $g$-force analysis of following this route at the desired Hyperloop speeds was shown to be problematic as lateral $g$-force exceeded $0.5g$ and accelerations changed rapidly. Land will need to be acquired to smooth the track path and maintain passenger comfort. Although this is not predicted to be an issue in the middle section of the journey, many obstacles can arise in the suburban area due to existing infrastructure and community pressures. Alternative solutions can be considered, but ultimately costs for acquiring land will be much higher than the alpha document estimated.

Civil infrastructure costs make up the largest percentage of total capital costs and they were determined to be underestimated based on material cost analysis, review of other large-scale infrastructure projects, custom pylon manufacturing requirements, and higher tunneling costs. After a detailed revision, the estimated capital costs of the Hyperloop were determined to be \$16.84 billion dollars, nearly three times the cost of the alpha proposed \$6 billion. Still, this cost is well beneath the projected \$68.4 billion of the California High Speed Rail System. Some of the revised costs may still be conservative because several technological components have not been proven on a large scale, and at this early stage there are many other unknowns and unaccountable factors that will increase final cost. Even if the Hyperloop goes over

budget by the average amount of 45% for a large-scale infrastructure project, it is still well below the California High Speed Rail's projected costs. The high speed rail offers minimal transportation improvements and technological advancements, and it is not worth the massive investment. Therefore, if investments and demand are high enough to build a transportation system between Los Angeles and San Francisco it is recommended to go ahead with the Hyperlooop instead of the high speed rail. The benefits of investing in the Hyperloop will impact more than just the people of California. Large-scale transportation has become stagnant and the Hyperloop can ignite a new wave in transportation innovations throughout the world. The possibility of one day connecting any two major cities across the world by less than a couple hour capsule ride is inspiring.

# Bibliography


[1] Luke Abaffy. Can Engineers Make Hyperloop a Reality? *Engineering News-Record*, (September):2–4, 2013.

[2] John Anderson. *Fundamentals of Aerodynamics*. McGraw-Hill Education, 5 edition, 2010.

[3] Laurence Blow. Maglev Technology Costs for Transrapid Vehicle System. Technical report, MaglevTransport, Inc., 2002.

[4] Matt Brauer and Guy Rouleu. Hyperloop: Not so fast!, 2013.

[5] Richard G. Budynas and J. Keith Nisbett. *Shigley's Mechanical Engineering Design*. McGraw-Hill, New York, 9 edition, 2011.

[6] Bureau of Labor Statistics. Average Energy Prices, Los Angeles-Riverside-Orange County, 2014.

[7] Y. Cai and S.S. Chen. Control of Maglev Suspension Systems. *Journal of Vibration and Control*, 2(3):349–368, January 1996.

[8] California High-Speed Rail Authority. California High-Speed Rail Program Revised 2012 Business Plan. Technical Report April, 2012.

[9] California High-Speed Rail Authority. California High-Speed Rail Project Cost Changes from 2009 Report to 2012 Business Plan Capital Cost Estimates. Technical Report April, 2012.

[10] California-Nevada Super Speed Train Commission and American Magline Group. California-Nevada Interstate Maglev Project ( CNIMP ) A Guideway to the Future. Technical report, American Magline Group, 2008.

[11] William D. Callister and David G Rethwisch. *Fundamentals of Materials Science and Engineering: An Integrated Approach*. Wiley, Hoboken, NJ, 4 edition, 2012.

[12] Cornell University Global Labor Institute. Pipe dreams ? Jobs Gained, Jobs Lost By the Construction of Keystone XL. Technical Report 5, Cornell University, 2011.

[13] Ginés de Rus. The Economic Effects of High Speed Rail Investment, 2012.

[14] Sandeep Dhamaja. Power from Regenerative Braking. In *Electrical Vehicle Battery Systems*, chapter Electric V, pages 43–68. Newnes: Butterworth-Heinemann, Boston, 2002.

[15] J. Patrick Donohoe. Induction (Asynchronous) Machines, 2010.

[16] Mohamed M Elmadany and Zuhair S Abduljabbar. Vehicle System Dynamics : Linear Quadratic Gaussian Control of a Quarter-Car Suspension Linear Quadratic Gaussian Control of a Quarter-Car Suspension. *International Journal of Vehicle Mechanics and Mobility*, (September):37–41, 2010.

[17] Keith A. Escoe. An Introduction to Engineering Mechanics of Piping. In *Piping and Pipeline Assessment Guide*, chapter 2. Gulf Professional Publishing, Oxford, 1 edition, 2006.

[18] Bent Flyvbjerg, Mette Skamris Holm, and Sø ren Buhl. Cost Underestimation in Public Works Projects: Error or Lie? *Journal of the American Planning Association*, 68(3), 2002.

[19] R.L. Forgacs. Evacuated tube vehicles versus jet aircraft for high-speed transportation. *Proceedings of the IEEE*, 61(5):604–616, 1973.

[20] Nick Garzilla. The Transportation Innovation Act, 2014.

[21] Bhag S. Guru and Hüseyin R. Hizirolu. Linear Induction Motor. In *Electric Machinery and Transformers*, pages 678–685. Oxford University Press, 3 edition, 2001.

[22] William H. Heiser and David T. Pratt. Freestream Knudsen Number. In *Hypersonic Airbreathing Propulsion*, chapter 2. AIAA Educaation Series, Washington, D.C., 1994.

[23] João P. Hespanha. *Linear Systems Theory*, volume 4. Princeton University Press, Princeton, 2009.

[24] R. C. Hibbeler. *Mechanics of Materials*. Pearson Prentice Hall, Boston, 8 edition, 2011.

[25] Andrew P Johnson. *High Speed Linear Induction Motor Efficiency Optimization*. PhD thesis, Massachusetts Institute of Technology, 2005.

[26] E.R. Laithwaite. *Induction Machines for Special Purposes*. Littlehampton Book Services Ltd, 1966.

[27] Hongyi Li, Xingjian Jing, and Hamid Reza Karimi. Output-Feedback-Based H Control for Vehicle Suspension Systems With Control Delay. *IEEE Transactions on Industrial Electronics*, 61(1):436–446, 2014.

[28] Qing Ling Li, Wen Guang Jia, Chen Guang Dong, and Rui Xiang Duan. Numerical Research of Thermal-Pressure Coupling Effect on Blockage Ratio in the Evacuated Tude Transportation System. *Key Engineering Materials*, 561:454–459, July 2013.

[29] Jiaqing Ma, Dajing Zhou, Lifeng Zhao, Yong Zhang, and Yong Zhao. The approach to calculate the aerodynamic drag of maglev train in the evacuated tube. *Journal of Modern Transportation*, 21(3):200–208, September 2013.

[30] MathWorks. Active Suspension Control Design - MATLAB & Simulink, 2013.

[31] MathWorks. H-Infinity Synthesis - MATLAB & Simulink, 2013.

[32] Robert D. Mead. *Journeys Down the Line: Building the Trans-Alaska Pipeline*. Doubleday, 1978.

[33] Michael J. Moran and Howard N. Shapiro. *Fundamentals of Engineering Thermodynamcis*. Wiley, Hoboken, NJ, 6 edition, 2008.

[34] Elon Musk. Hyperloop Alpha. Technical report, SpaceX, 2013.

[35] National Academy of Engineering, National Research Council, and Transportation Research Board of the National Academies. Completing the "Big Dig": Managing the Final Stages of Boston's Central Artery/Tunnel Project. Technical report, The National Academies Press, Washington, D.C., 2003.

[36] Oerlikon Leybold Vacuum. Fundamentals of Vacuum Technology, 2007.

[37] Daryl Oster. Rail vs. ETT, 2010.

[38] Daryl Oster, Masayuki Kumada, and Yaoping Zhang. Evacuated Tube Transport Technologies (ET3): a maximum value global transportation network for passengers and cargo. *Journal of Modern Transportation*, 19(1):42–50, 2011.

[39] Greg Paula. Evaluation EPACT's Impact. *Mechanical Engineering Magazine*, (June), 1998.

[40] Pfieffer Vacuum. CombiLine WU Data Sheet. Technical report, Germany, 2009.

[41] Pfieffer Vacuum. Vacuum Technology Know How. Technical report, Germany, 2009.

[42] Don Plotkin and Simon Kim. Maglev Guideway Cost and Construction Schedule Assessment. *Journal of Transportation Engineering*, (195), 1997.

[43] Robert W. Pratt. Pilot-induced oscillations (PIOs). In *Flight Control Systems: practical issues in design and implementation*, chapter 4, pages 150–167. TJ International, Padstow, Cornwall, 2000.

[44] Pro SwissMetro. SwissMetro - Technology, 1995.

[45] Giuseppe Quaglia and Massimo Sorli. Air Suspension Dimensionless Analysis and Design Procedure. *Vehicle Systems Dynamics*, 35(6), 2001.

[46] Road Traffic Technology. Boston Big Dig, Central Artery/Tunnel Project. *Massacusetts - Road Traffic Technology*, 2013.

[47] Sami Roinila. *H Control Design of an Active Vehicle*. PhD thesis, Tampere University of Technology, 2011.

[48] R. M. Salter. The Very High Speed Transit System. Technical report, Rand Corporation, 1972.

[49] Olivier Sename and Luc Dugard. Robust H-Infinity Control of Quarter-Car Semi-Active Suspension.

[50] Xu Shuo, Zhou Ke, Luo Zhe, and Yu Fan. Study of PID Control for a Semi-Track Air-Cushion Vehicle Based on Power Consumption Optimization. *Institute of Electrical and Electronics Engineers*, 2006.

[51] Siemens, ThyssenKrupp, and Transrapid International. High-Tech for Flying on the Ground . Technical report, Transrapid International, Berlin, 2002.

[52] Hebertt Sira-Ramirez and Carlos A. Ibanez. The Control of the Hovercraft System : A Flatness Based Approach. In *International Conference on Control Applications*, Anchorage, Alaska, 2000. IEEE.

[53] Alexander J. Smits. *A Physical Introduction to Fluid Mechanics*. John Wiley, Princeton, 2 edition, 2012.

[54] Sandeep Sovani. Bringing the Hyperloop One Step Closer to Reality Through Simulation, 2013.

[55] R. L. Strykowsky, T. Brown, M. Cole Chrzanowski, P. Heitzenroeder, G. H. Neilson, Donald Rej, and M. Viola. Engineering Cost & Schedule Lessons Learned On NCSX. Technical report, Princeton Plasma Physics Laboratory, Princeton, 2014.

[56] Antoni Szumanowski. Energy Efficiency of Regenerative Braking. In *Hybrid Electric Power Train Engineering and Technology - Modeling, Control, and Simulation*, chapter 10, pages 381–405. Engineering Science References, Hershey, PA, 2013.

[57] W. J. Thayer. Transfer Functions for MOOG Servovalves. Technical report, MOOG Inc., East Aurora, NY, 1965.

[58] Transportation Research Board of the National Academies. *Transit Capacity and Quality of Service Manual*. Federal Transit Administration, Washington, D.C., 2 edition, 2003.

[59] U.S. Department of Transportation: Research and Innovative Technology Administration. Transportation Fatalities by Mode. Technical report, Bureau of Transportation Statistics, 2012.

[60] U.S. Geological Survey. The Trans-Alaska Pipeline Survives the Quake - A Triumph of Science and Engineering, 2003.

[61] D. M. Van Wie, F. T. Kwok, and R. F. Walsh. Starting Characteristics of Supersonic Inlets. *American Institute of Aeronautics and Astronautics*, (July), 1996.

[62] Yao Ping Zhang. Explicit Formula for Estimating Aerodynamic Drag on Trains Running in Evacuated Tube Transportation. *Applied Mechanics and Materials*, 307:156–160, February 2013.

[63] Yao Ping Zhang and Daryl Oster. Study on Materials and Structure of the Tube Wall of Evacuated Tube Transportation. *Advanced Materials Research*, 487:582–587, March 2012.

[64] Yaoping Zhang. Vehicle scheme of Evacuated Tube Transportation in the future logistics system. *2010 The 2nd International Conference on Computer and Automation Engineering (ICCAE)*, 5:190–192, February 2010.

[65] Yaoping Zhang. Evacuated Tube Transportation Routes: Going Overheard, At Ground Level, Shallow Underground or Deeply Underground?, 2013.

[66] Yaoping Zhang. Numerical simulation and analysis of aerodynamic drag on a subsonic train in evacuated tube transportation. *Journal of Modern Transportation*, 20(1):44–48, September 2013.

[67] Yaoping Zhang, Daryl Oster, Masayuki Kumada, Jianye Yu, and Shengshan Li. Key vacuum technology issues to be solved in evacuated tube transportation. *Journal of Modern Transportation*, 19(2):110–113, September 2013.

[68] Yaoping Zhang, Jianyue Yu, Maoxing Shen, Daryl Oster, and Chen Chen. Affecting factors and numerical value calculation relating to vacuumizing time in Evacuated Tube Transportation. *Proceedings of 2011 6th International Forum on Strategic Technology*, 7:246–249, August 2011.

[69] Yaoping Zhang, Jun Zhu, Baigang Mi, and Maoxing Shen. Reasonable Figure of Subsonic Train Front and Rear in Evacuated Tube Transportation Based on Aerodynamics Consideration. *Proceedings of the 2nd International Conference on Electronic and Mechanical Engineering and Information Technology (2012)*, pages 734–739, 2012.

[70] Y.P. Zhang, S.S. Li, and M.X. Wang. Main Vacuum Technical Issues of Evacuated Tube Transportation. *Physics Procedia*, 32:743–747, January 2012.

# Appendix A

# Important System Parameters

The following important system parameters were derived from the Hyperloop alpha document and were used throughout the analysis of the Hyperloop's subsystems.

## Fluid Flow Parameters

There are three cruising speeds the Hyperloop capsule will operate at.

$u_{e,\,max} = 339.75\ \ m/s$ (Maximum capsule speed)

$u_{e,\,mid} = 248.11\ \ m/s$ (Middle capsule speed)

$u_{e,\,low} = 134.11\ \ m/s$ (Low capsule speed)

## Capsule Parameters

$m_c = 15000\ \ kg$ (Mass of Passenger Capsule including passengers and luggage)

$L_{capsule} = 31\ \ m$ (Length of Passenger Capsule)

$H_{capsule} = 1.1\ \ m$ (Maximum Passenger Capsule Height)

$W_{capsule} = 1.35\ \ m$ (Maximum Passenger Capsule Width)

$SA_{c,\,front} = 1.4\ \ m^2$ (Passenger Capsule Frontal Surface Area)

$SA_{c,\,bottom} = 41.85\ \ m^2$ (Passenger Capsule Bottom Surface Area)

## Tube Parameters

$T_\infty = 293.15\ K$ (Temperature of Air in Surrounding Tube)

$\mu_\infty = 1.8369247e^{-5}\ \frac{N-s}{m^2}$ (Viscosity of Air in Tube)

$\gamma = 1.4$ (Adiabatic Index)

$R_{air} = 287\ \frac{J}{kg-K}$ (Gas Constant Air)

$p_{tube} = 100\ Pa$ (Tube Pressure)

$\rho_\infty = \frac{p_{tube}}{R_{air}\,T_\infty} = 0.001188579\ \frac{kg}{m^3}$ (Density of Air in Tube)

$D_{tube} = 2.23\ m$ (Passenger Tube Diameter)

$SA_{tube} = \pi\left(\frac{D_{tube}}{2}\right)^2 = 3.9057\ m^2$ (Passenger Tube Surface Area)

$t_{tube} = 23.0\ mm$ (Passenger Tube Thickness)

## Propulsion Parameters

$d_{prop} = 4\ km$ (Length of Propulsion Track)

$a_{1g} = 9.81\ m/s^2$ ($1g$ Propulsion Acceleration)

## Suspension Gap Parameters

$h_{gap,\,max} = 0.5\ mm$ (Maximum Suspension Gap Height)

$h_{gap,\,min} = 1.3\ mm$ (Minimum Suspension Gap Height)

$T_{gap} = 398.15\ K$ (Temperature of Air in Gap)

$\mu_{gap} = 2.31849e^{-5}\ \frac{N-s}{m^2}$ (Viscosity of Air in Gap)

$p_b = 9400\ Pa$ (Bearing Pressure)

$\rho_{gap} = \frac{p_b}{R_{air}\,T_{gap}} = 0.08226199\ \frac{kg}{m^3}$ (Density of Air in Gap)

## Air Suspension Bearing Parameters

$L_{ski} = 1.5\ m$ (Bearing Ski Length)

$W_{ski} = 0.9\ m$ (Bearing Ski Width)

$\alpha = 0.05^{\circ}$ (Angle of Attack)

$N_{ski} = 28$ (Number of Air Bearing Skis)

$SA_{ski} = L_{ski} W_{ski} = 1.35\ m^2$ (Bearing Ski Surface Area)